Compositions of anhydrous and hydrous melts coexisting with plagioclase, augite, and olivine or low-Ca pyroxene from 1 atm to 8 kbar: Application to the Aleutian volcanic center of Atka

Don R. Baker,[1] **David H. Eggler**

Department of Geosciences, Pennsylvania State University, University Park, Pennsylvania 16802, U.S.A.

Abstract

Phase relations and partial melt compositions have been determined for a suite of high-alumina basalts and andesites from the Aleutian island of Atka and from the Mariana islands. Experimental conditions varied from anhydrous, at pressures from 1 atm to 8 kbar, to hydrous (2% H_2O in the melt) at 2 and 5 kbar, although not all compositions were studied at all conditions.

Partial melt compositions at 1 atm, projected onto pseudoternary phase diagrams, define phase fields for plagioclase, augite, olivine, and orthopyroxene. Hydrous partial melts, 2 wt% H_2O in the melt, at 2 and 5 kbar define equivalent phase fields. At all those conditions, the four phases coexist with melts of andesitic composition, and olivine reacts with those melts to produce orthopyroxene. Anhydrous partial melt compositions at 8 kbar, however, define phase fields for plagioclase, olivine, augite, and pigeonite. Phase compositions indicate the presence of thermal divides on both the plagioclase-olivine-augite and plagioclase-augite-pigeonite phase boundaries.

Crystallization fractionation at deep-crustal pressures of 8 kbar can only account for a portion of Atka basalt compositions, but it cannot account for the total array of Atka rock compositions, because of the presence of a thermal divide involving pigeonite cyrstallization. Even though the olivine reaction relation has been demonstrated to occur, lower-pressure anhydrous fractionation cannot account for andesitic and dacitic melts. In reality, all Atka rock compositions are considerably more aluminous (more plagioclase-rich on pseudoternary diagrams) and less Fe-enriched than low- or high-pressure anhydrous multiply saturated melts. That mismatch can be alleviated, at least for andesites and dacites, on the hypothesis that andesite and dacite melts containing about 2% H_2O have evolved from basaltic andesite parents in crustal magma chambers (2–5-kbar pressure). The array of Atka basalt to andesitic basalt compositions is also consistent with crystallization fractionation at 5–8-kbar pressures and low H_2O contents, although experimental details are currently lacking.

Introduction

Andesites may represent partial melts of either mantle peridotite (Mysen, 1982) or subducted oceanic slab (Green and Ringwood, 1968), mixing of basaltic and dacitic magmas (Eichelberger, 1975), contamination of basaltic magmas by crustal rocks, or crystallization fractionation of basaltic magmas. Both hydrous (Kay et al., 1982) and anhydrous (Osborn, 1959, 1979; Gill, 1981) fractionating crystal assemblages have been proposed. The former assemblage contains hornblende (Kay et al., 1982). Amphibole is, however, a rare phenocryst in andesitic rocks from oceanic island arcs (Gill, 1981; Ewart, 1982; Marsh, 1982), but is more common in andesitic rocks erupted through continental crust (Coulon and Thorpe, 1981;

Ewart, 1982; Leeman, 1983). The anhydrous assemblage consists of plagioclase, olivine, clinopyroxene, and possibly magnetite (Gill, 1981).

Hydrous experiments performed at crustal pressures have primarily investigated amphibole crystallization in rocks of basaltic composition (Holloway and Burnham, 1972; Helz, 1976; Cawthorn, 1976; Cawthorn et al., 1973; Allen et al., 1975; Allen and Boettcher, 1978) with water contents greater than approximately 4 wt%. Experimental results provide some support for the hydrous crystallization fractionation hypothesis, although, unlike most andesites, experimentally produced andesitic melts are typically peraluminous (Ewart, 1982).

Anhydrous crystallization fractionation has been investigated by Grove et al. (1982) and Grove and Bryan (1983); these investigators located a reaction point at 1 atm involving olivine, augite, plagioclase, pigeonite, and

---

[1] Present address: Department of Geology, Rensselaer Polytechnic Institute, Troy, New York 12180-3590, U.S.A.

Table 1. Compositions of basalts and andesites studied

	AT-1†	AT-112†	AT-41†	AT-29†	AT-25†	M-46†	AG8-4‡	AG7-1‡	P-22§
SiO$_2$	50.4	49.0	54.7	56.8	57.2	52.4	57.4	60.1	51.6
TiO$_2$	1.29	1.02	0.79	1.01	0.92	1.33	0.88	0.81	2.05
Al$_2$O$_3$	19.7	19.0	18.7	16.9	17.1	14.5	15.9	16.0	15.0
FeO*	9.08	9.47	7.90	8.03	6.98	13.0	9.86	8.80	11.7
MnO	0.28	0.21	0.31	0.17	0.21	0.43	0.22	0.22	0.22
MgO	5.05	6.18	3.29	3.09	3.32	4.30	2.41	1.87	5.30
CaO	9.59	11.4	7.96	7.05	7.07	9.03	6.29	5.81	10.76
Na$_2$O	3.42	2.56	4.10	3.99	3.90	3.15	3.88	4.25	3.02
K$_2$O	0.79	0.65	0.99	2.05	2.47	0.85	1.88	2.06	0.52
P$_2$O$_5$	0.31	0.11	0.25	0.28	0.16		0.28	0.35	0.0
Total	99.91	99.60	98.99	99.37	99.33	98.98	98.92	100.27	100.17

* All Fe determined as FeO.
† Microprobe analyses of superliquidus or near-liquidus glasses.
‡ XRF analyses from Stern (1979).
§ Microprobe analysis from Walker et al. (1979).

melt that apparently prevents basaltic compositions from producing andesitic residual melts by crystal fractionation.

To better understand andesite petrogenesis beneath the Aleutian island of Atka, compositions of partial melts of high-alumina basalts and andesites were determined at pressures from 1 atm to 8 kbar under anhydrous conditions and from 2 to 5 kbar at water-undersaturated conditions, extending the study of Baker and Eggler (1983).

SAMPLE DESCRIPTION AND PREPARATION

Sample description

Rocks studied represent a suite of high-alumina basalts and andesites from the Aleutian island of Atka (Marsh, 1982), various islands in the Mariana island arc, and one sample from the Oceanographer fracture zone (Table 1).

Atka rocks. Samples AT-1, AT-112, and AT-41, which are similar to other high-alumina basalts (Kuno, 1960), all contain phenocrysts of plagioclase, olivine, and magnetite; AT-41 also has phenocrysts of clinopyroxene. Samples AT-25 and AT-29, which are typical oceanic island arc andesites (Ewart, 1982), contain phenocrystic plagioclase, clinopyroxene, and orthopyroxene.

Mariana and Oceanographer fracture zone rocks. The basalt from the Marianas, M-46-10B (hereafter referred to as M-46), is from Esmerelda Bank (Dixon and Stern, 1983), a seamount that lies behind the volcanic arc. The andesites, AG7-1 and AG8-4, are from the island of Agrigan (Stern, 1979) and are typical of the andesites found in the Marianas (Dixon and Batiza, 1979). The Oceanographer fracture zone rock is a tholeiitic basalt, P-22; 1-atm melting experiments have previously been performed on this rock by Walker et al. (1979).

Mineral separates. Mineral separates (Table 2) were used in "forced saturation" experiments. Minerals used were olivine from the Duke Island ultramafic complex of southeast Alaska (Irvine, 1974), plagioclase from Crystal Bay, Minnesota (U.S. National Museum no. R2912), and augite from the Frosty Peak volcanic complex on the Alaskan Peninsula (collected by D.R.B.). Analyses of these minerals are presented in Table 2.

Sample preparation

Rock samples. Rocks were received as chips (AT-1, AT-25, AT-29, AT-41, AT-112, P-22) or as powder of approximately −200 mesh (M-46, AG7-1, AG8-4). Rock chips were crushed

and ground in a tungsten carbide–lined ball mill until greater than 75% of the grains were less than 5 μm in their longest dimension (Baker, 1985). Rock powders were stored in either a drying oven or dessicator.

Mineral separates. Mineral separates were crushed in a percussion mortar and ground for 1 to 2 h under ethanol with an agate mortar and pestle. The size fraction less than 400 mesh was used to make starting mixes. Mixes of combined mineral separates were then ground together for 1 h under ethanol with an agate mortar and pestle and stored in either a drying oven or dessicator.

EXPERIMENTAL TECHNIQUES

Anhydrous experiments

One-atmosphere experiments. One-atmosphere experiments were performed in either silicon carbide–heated (Pennsylvania State University) or platinum-wound (Smithsonian Institution, experiments 3, 4, 11, and 14) gas-mixing furnaces in which CO$_2$ and H$_2$ gases were used to control the oxygen fugacity. Rocks were melted on pretreated Pt loops (Baker and Eggler, 1983; Baker, 1985). Other experimental techniques were the same as Mahood and Baker (1986) with the exception that all experiments were performed within 0.3 log units of the nickel–nickel oxide buffer (NNO).

Durations of experiments varied from a few hours at near-liquidus temperatures to 480 h at 1060°C. Experiments of 24- and 480-h duration at 1060°C on andesite AT-29 did not vary

Table 2. Compositions of mineral separates

	Olivine†	Plagio-clase‡	Augite‡
SiO$_2$	37.1	49.7	50.2
TiO$_2$	0.0	0.06	0.81
Al$_2$O$_3$	0.2	31.0	3.56
FeO*	17.4	0.40	7.86
MnO	0.1	0.12	0.24
MgO	44.2	0.04	14.7
CaO		15.3	21.1
Na$_2$O	0.3	2.47	0.24
K$_2$O	0.0	0.07	0.0
Total	99.3	99.16	98.71

* All Fe determined as FeO.
† Analysis from Irvine (1974).
‡ Microprobe analysis.

in melt composition and phase assemblage (App. Table 1, experiments 11 and 14), indicating that andesites and basalts can reach steady state, if not equilibrium, with respect to both phase assemblage and melt composition within 24 h.

Solid media apparatus experiments. Experiments at 8 kbar and higher pressures were performed in a single-stage solid media apparatus (Boyd and England, 1960). Talc–Pyrex–crushable alumina assemblies, 2.54-cm diameter, were used. Graphite capsules inside 3-mm Pt capsules were used to contain rock powders in all experiments for which partial melt compositions were determined (App. Table 1). Loaded capsules were dried at 110°C for 1 h and fired to red heat for 30 s before welding. Further details of encapsulation techniques and pressure-temperature control are discussed in Baker (1985) and Mahood and Baker (1986).

Runs at 8 kbar varied in duration from 1 h near 1300°C to 196 h near 1100°C. Experiments performed by partially melting rock powders ("melting experiments") or by completely melting rock powders and then lowering the temperature to the same temperature as the partial melting experiments ("crystallization experiments") produced the same phase assemblage and similar phase compositions for rocks AT-1 (App. Table 1, experiments 891 and 953) and AT-29 (App. Table 1, experiments 1010 and 989). These experiments suggest close approach to equilibrium although near-solidus phase proportions and compositions produced in different experiments on rock AT-112 were inconsistent (App. Table 1, experiments 940 and 1098).

For the 8 kbar "forced saturation" experiments, rock powders were placed between layers of a plagioclase-augite-olivine mixture (Takahashi and Kushiro, 1983; Baker, 1985). A series of variable duration experiments, 24 to 96 h at 1200°C, produced somewhat variable melt compositions (App. Table 1), apparently due to inhomogeneous Fe distribution in starting materials; nevertheless, melts appear to reach a steady-state composition within 24 h (Baker, 1985).

Hydrous experiments

Internally heated pressure vessel techniques. Experiments were performed at 2 and 5 kbar in internally heated pressure vessels (Holloway, 1971). Temperature was monitored with two Pt-$Pt_{90}Rh_{10}$ thermocouples calibrated against an NBS-certified thermocouple and held within 5 deg of the desired temperature. The thermal gradient along the samples was below 3 deg. No pressure correction was made on the thermocouple emf. Pressures, monitored with manganin cells, were precise to 60 bars and believed accurate to 100 bars. Oxygen fugacity was controlled within 0.7 log units of NNO by controlling H_2 partial pressure using a Pt membrane; this technique was checked against NNO and fayalite-magnetite-quartz (FMQ) buffer capsules containing H_2O-CO_2 mixtures (Baker, 1985). Experiments were quenched at approximately 500°C/min.

Capsules were 3-mm diameter and either $Ag_{50}Pd_{50}$ or Pt, which were treated with wüstite (Helz, 1978; Baker, 1985) in order to mitigate Fe loss from the samples. Despite these precautions, Fe loss occurred in the 2- and 5-kbar experiments (App. Table 1).

"Melting experiments" were at 2 and 5 kbar, except for one forced-saturation experiment. Experiments varied in duration from 2 h at superliquidus conditions to 96 h at temperatures near 1000°C. In experiments performed on AT-25 and AT-29 at 1020°C for both 24- and 96-h duration, the phase assemblage was the same and compositions of AT-25 partial melts (App. Table 1, experiments 1147 and 1248) were similar. Compositions of AT-29 partial melts were different (App. Table 1, ex-

periments 1148 and 1174), presumably as the result of variable amounts of Fe absorption by the capsule.

Control and calculation of H_2O contents of experimentally produced melts. H_2O contents of experimentally produced melts were controlled by changing compositions of H_2O-CO_2 fluids present in experiments (cf. Eggler, 1972; Baker and Eggler, 1983). Capsules were loaded with oxalic acid dihydrate and silver oxalate in correct proportions to yield a fluid with mole fraction of H_2O near 25% (2-kbar experiments) or 18% (5-kbar experiments). Fluid weight was kept approximately equal to rock powder weight to minimize changes in the fluid composition due to differential melt solubilities of H_2O and CO_2 (Holloway, 1976). Capsules were welded with no loss of volatiles.

After each experiment capsules were weighed; many capsules were very brittle due to Fe absorption and lost fluid during quench. The fluid H_2O:CO_2 ratio in unfailed capsules was determined by a weight-loss technique (Baker and Eggler, 1983).

For capsules that did not fail, H_2O contents of melts can be calculated from fluid compositions by assuming H_2O activity–composition models for silicate melts (Burnham, 1979, 1981) and for H_2O-CO_2 fluids. An ideal-mixing model was used for fluids, in part because the system quartz-sanidine-H_2O-CO_2 suggest near-ideality (Bohlen et al., 1983) and in part because a more complicated Redlich-Kwong model (Holloway, 1977, pers. comm.) yields nearly identical activities.

For failed capsules, H_2O contents can still be calculated by iterating the above procedure with the constraint of mass balance (Merzbacher and Eggler, 1984; Baker, 1985). The iterative procedure can also be performed for the subset of capsules that did not fail, serving as a check of the melt and fluid activity-composition models and measurement techniques. In that check, measured and calculated fluid compositions are entirely comparable.

As a test of these techniques, the liquidus of AT-1 +2.5 wt% H_2O was determined at 8 kbar in the solid media apparatus, both when H_2O was added directly and when silver oxalate + H_2O was added in the correct proportions to produce a melt with the desired H_2O content. Agreement of the liquidus determinations, within 10 deg, for both methods of H_2O addition indicates an uncertainty of 0.35 wt% in the calculated H_2O content of the melt.

Analytical techniques

Selected run products were analyzed by electron microprobe, at Pennsylvania State University and the National Museum of Natural History, Smithsonian Institution, at 15-kV accelerating potential and 0.012-μA sample current using the data-reduction techniques of Bence and Albee (1968) with matrix-correction factors of Albee and Ray (1970).

Run products were imaged using SEM attachments on microprobes, and crystals were analyzed with a 2-μm beam. Olivines and most pigeonites were compositionally homogeneous. Augite and plagioclase crystals were invariably heterogeneous, even in crystallization experiments. Except where quench overgrowths on the rims of crystals were observed, rim compositions (analyses made 5–15 μm from the rim of the crystal) are presented. Quench overgrowths were only apparent (by secondary-electron imaging and quantitative analyses) in a few experiments performed in the internally heated vessel.

To minimize alkali loss during analysis, 10–20-μm diameter beams were used to analyze glass in run products wherever possible. Comparison between microprobe analyses of AT-29 and AT-25 superliquidus glasses and wet chemical analyses (B. D.
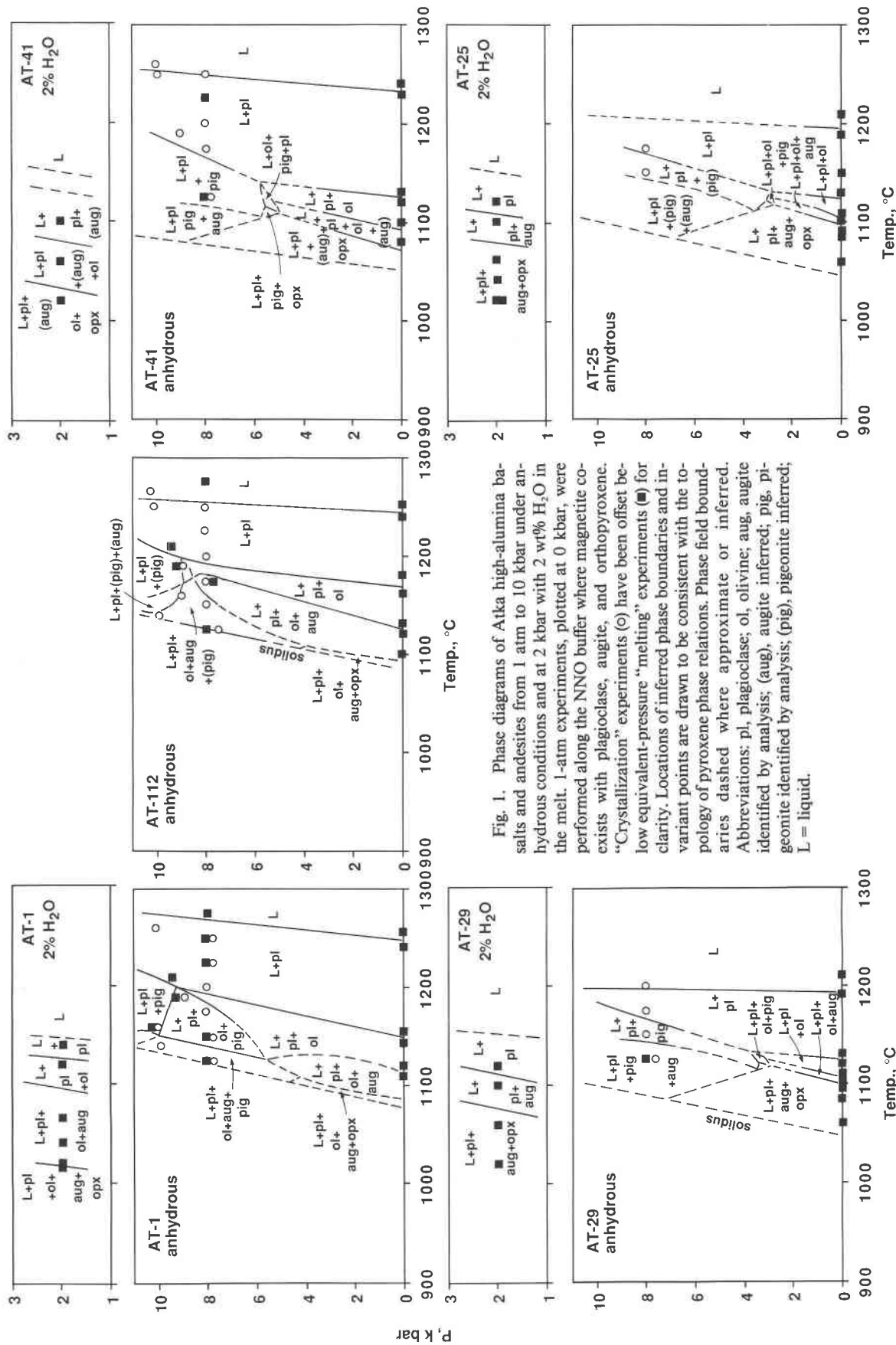
Fig. 1. Phase diagrams of Atka high-alumina basalts and andesites from 1 atm to 10 kbar under anhydrous conditions and at 2 kbar with 2 wt% H_2O in the melt. 1-atm experiments, plotted at 0 kbar, were performed along the NNO buffer where magnetite coexists with plagioclase, augite, and orthopyroxene. "Crystallization" experiments (○) have been offset below equivalent-pressure "melting" experiments (■) for clarity. Locations of inferred phase boundaries and invariant points are drawn to be consistent with the topology of pyroxene phase relations. Phase field boundaries dashed where approximate or inferred. Abbreviations: pl, plagioclase; ol, olivine; aug, augite identified by analysis; (aug), augite inferred; pig, pigeonite identified by analysis; (pig), pigeonite inferred; L = liquid.

Marsh, pers. comm., 1980) indicate the success of using these large-diameter beams in minimizing, or even eliminating, alkali loss.

Weight percent modes of some experiments were calculated using bulk-rock compositions and the compositions of run-product phases as input to a least-squares mixing program (Bryan et al., 1969). Fe loss in hydrous experiments was calculated by using wüstite as a potential phase. Modes for such experiments were corrected for Fe loss by normalization of silicate modes to a total free of modal wüstite.

EXPERIMENTAL RESULTS

Compositions of multiply saturated melts and coexisting crystals at pressures from 1 atm to 8 kbar are listed in Appendix 1. Additional experimental data used for the construction of phase diagrams are presented in Baker (1985).

Anhydrous phase relations

High-alumina basalts. High-alumina basalts AT-1, AT-41, and AT-112 have similar phase relations (Fig. 1), except for the lack of clinopyroxene in the 1-atm phase relations of AT-41. At 1 atm along the NNO buffer, plagioclase is the liquidus phase followed by olivine, then clinopyroxene. The clinopyroxene that crystallizes from AT-1 and AT-112 compositions is an augite. At 8-kbar, plagioclase remains the liquidus phase for all compositions studied. The plagioclase liquidus for AT-1 in "crystallization experiments" was 25 deg below the liquidus temperature of plagioclase in "melting experiments," probably due to inhibited plagioclase nucleation at near-liquidus temperatures (Gibb, 1974).

The 1-atm clinopyroxene that crystallized from AT-1 is augite ($Wo_{39}En_{42}Fs_{19}$; Baker and Eggler, 1983), whereas at 8 kbar, pigeonite ($Wo_{12}En_{63}Fs_{24}$) crystallized. Pigeonite ($Wo_{10}En_{50}Fs_{40}$) also crystallized from AT-41 at 8 kbar. Clinopyroxene that crystallized from AT-112 at 8 kbar is on the boundary between augite and subcalcic augite ($Wo_{25}En_{56}Fs_{18}$). Changes in pyroxene chemistry in AT-1 are due to the expansion of the low-Ca pyroxene primary phase field, relative to augite, as pressure increases (cf. Kushiro, 1969).

Andesites. At 1 atm, Atka andesites AT-25 and AT-29 exhibit similar phase relations (Fig. 1): plagioclase followed by olivine and augite ($Wo_{39}En_{43}Fs_{19}$ in AT-29). Orthopyroxene and magnetite join the sequence, and olivine disappears at temperatures near 1100°C.

At 8 kbar, plagioclase is still the liquidus phase for AT-29 (Fig. 1), but crystallizes at approximately 1163°C, a temperature below the 1-atm plagioclase liquidus. This discrepancy is attributed to difficulties in plagioclase nucleation; the estimated 8-kbar plagioclase melting temperature is 1190°C. At 1125°C, plagioclase, melt, and two clinopyroxenes ($Wo_{14}En_{55}Fs_{31}$ and $Wo_{24}En_{46}Fs_{30}$) coexist; this phase assemblage is present in both "melting" and "crystallization" experiments at 1125°C. Because microprobe analyses were only made of AT-29 run products, it is not known which clinopyroxene(s) is present in AT-25 at 1150°C.

At 8 kbar, plagioclase is the liquidus phase (at approximately 1190°C) for Agrigan andesites AG7-1 and AG8-4 followed by pigeonite ($Wo_9En_{53}Fs_{38}$, ~1160°C). These minerals crystallize from AG7-1 and AG8-4 to the lowest temperatures investigated at 8 kbar (1050°C).

Hydrous phase relations

Previously published phase relations of high-alumina basalt AT-1 at 2 kbar (Baker and Eggler, 1983) are here supplemented by experiments on Atka rock compositions at 2 and 5 kbar with ~2 wt% H_2O in the melt. Owing to variable Fe loss, phase relations determined in this study are approximate, and melting temperatures of mafic phases should be considered as maxima.

The liquidus mineral of AT-1 and AT-41 at 2 kbar and 2 wt% H_2O is plagioclase (Fig. 1), followed by olivine (AT-1) or augite (AT-41, $Wo_{39}En_{49}Fs_{13}$). (Exact liquidus temperatures were not determined.) Orthopyroxene apparently crystallizes from both high-alumina basalts between 1030°C (AT-41) and 1020°C (AT-1). Andesites AT-25 and AT-29 also have plagioclase as the liquidus phase at 2 kbar (Fig. 1), followed by augite ($Wo_{40}En_{42}Fs_{18}$). AT-29 crystallizes orthopyroxene ($Wo_5En_{69}Fs_{27}$) but not olivine. AT-25 crystallizes olivine at 1080°C and possibly orthopyroxene at 1030°C. (Orthopyroxene was found in a 1020°C run in which greater than 50% of the original Fe content was lost to the capsule.)

Anhydrous liquid lines of descent

Compositions of a limited number of experimentally produced partial melts can be compared to a wide range of natural rock compositions (presumed to be *melt* compositions) in pseudoternary diagrams (O'Hara, 1968). This comparison has been very useful in elucidating the petrogenesis of mid-ocean ridge basalts (MORBs) (Walker et al., 1979; Grove and Bryan, 1983).

Pseudoternary diagrams used in this study (cf. Baker and Eggler, 1983) are a modification of the diagrams created by Walker et al. (1979). Baker and Eggler (1983) combined normative orthoclase with quartz as a "magmaphile" component (SiOr) enriched in residual melts, whereas Walker et al. (1979) combined orthoclase with plagioclase and Grove et al. (1982) used orthoclase as a component. In both cases, projection from Plag + Or or from Or incorrectly implies saturation of residual melts with orthoclase.

One-atmosphere liquid lines of descent. Compositions of partial melts (AT-25, AT-29, AT-41, and AT-112 at 1 atm along the NNO buffer, App. Table 1; Baker and Eggler, 1983; Eggler and Osborn, 1982), allow subdivision of a plagioclase-saturated pseudoternary diagram into fields of plag + ol, plag + aug, and plag + opx (Fig. 2).

At approximately 1100°C, olivine undergoes a reaction relation with the melt, wherein orthopyroxene and magnetite, without olivine, crystallize from andesitic bulk compositions AT-25 and AT-29. Melts coexisting with plag + aug + opx + mt are significantly enriched in silica and depleted in FeO*, compared to melts formed 20 deg
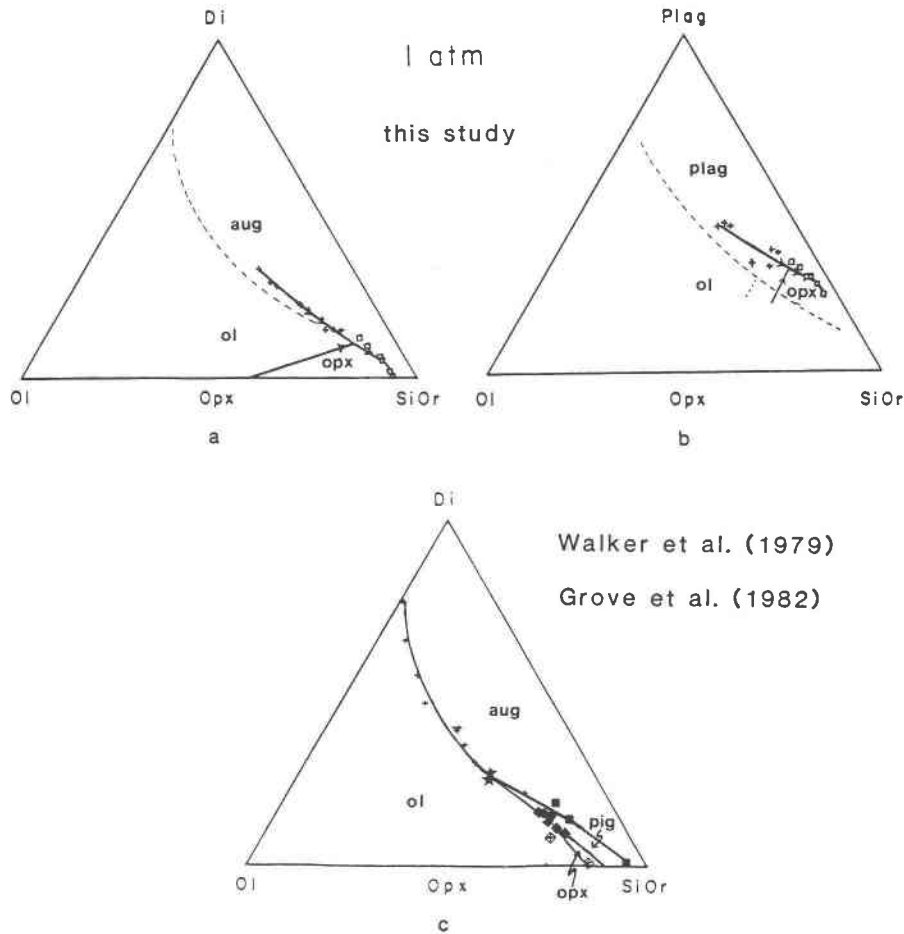
Fig. 2.   Pseudoternary diagrams at 1 atm. Pseudoternary diagrams constructed using the techniques of Baker and Eggler (1983) with the exception that the Qz + Or component has been renamed SiOr. (a) (Plag + Mt)–saturated pseudoternary with analyses of glasses produced in the 1-atm experiments along the NNO buffer. (b) (Di + Mt)–saturated pseudoternary diagram; +, glasses coexisting with plag + ol + aug; □, glasses coexisting with plag + aug + opx + mt. The long-dashed lines are the plag + ol + aug LLMSs determined by Walker et al. (1979) and Grove et al. (1982). The intersection of the short-dashed and long-dashed lines in Fig. 2b is the intersection of the plag + ol + opx LLMS and the plag + ol + pig LLMS determined by Grove et al. (1982). The arrows on the LLMS point in the direction of decreasing temperature. (c) (Plag + Mt)–saturated diagram based on the results of Walker et al. (1979) and Grove et al. (1982); +, melts coexisting with plag + ol + aug; ■, melts coexisting with plag + aug + pig; ⋆, melts coexisting with plag + ol + aug + pig, ◆, melts coexisting with plag + ol + pig; crosses within diamonds, melts coexisting with plag + ol + opx.

higher and coexisting with plag + ol + aug, presumably because of magnetite crystallization (Osborn, 1959, 1979).

The coexistence of augite, orthopyroxene, plagioclase, and andesitic melts (Fig. 2a) differs from the results of Grove et al. (1982) and Grove and Bryan (1983). These authors found that the plag + ol + aug liquid line of multiple saturation (LLMS) is terminated by a reaction point where ol + melt react to form pig + aug + plag. A field of pig + plag separates the fields of aug + plag and opx + plag (Fig. 2c). Grove et al. (1982) stressed that basaltic melts become trapped at the reaction point and do not undergo silica enrichment, but instead become enriched in Fe (cf. Fenner, 1931).

We attribute differences in phase diagrams (Figs. 2a, 2c) to differences in bulk compositions and in particular

to differences that are not displayed in pseudoternary diagrams. The two chief such differences are K$_2$O contents and Mg/(Mg + Fe^{2+}), which are plotted versus SiOr for the various LLMS (Fig. 3).

Values of Mg/(Mg + Fe^{2+}) in melts of this study are intermediate between values of Grove et al. and Walker et al. for equivalent phase assemblages, and hence Mg/(Mg + Fe^{2+}) differences are probably not significant. The relatively small (and overlapping) differences in Mg/(Mg + Fe^{2+}) also suggest that the slightly different oxygen fugacities in the sets of experiments (FMQ for Walker et al. and Grove et al.; NNO for this study) are not significant, because such differences should principally change Mg/(Mg + Fe^{2+}) of melts at any particular SiOr content.

It is apparent, however, that melts of Walker et al.

Table 3. Fe-Mg partitioning between crystals and melts at 1 atm and 2 kbar with f_{O_2} near the NNO buffer

	n*	$K_D =$ [(Fe$_{tot}$/Mg)$_{crystal}$]/ [(Fe$_{tot}$/Mg)$_{melt}$]	
		Mean	s.d.†
1 atm			
Olivine	4	0.29	0.03
Augite	9	0.21	0.05
Orthopyroxene	5	0.19	0.03
2 kbar			
Olivine	5	0.29	0.02
Augite	8	0.26	0.02
Orthopyroxene	2	0.25	0.04
2 kbar: experiment 1148			
Augite	1	0.17	
Orthopyroxene	1	0.18	
2 kbar: experiment 1174			
Augite	1	0.14	
Orthopyroxene	1	0.15	

* Number of experiments used to calculate the mean and standard deviation.
† One standard deviation of the calculated mean partition coefficient.

Fig. 3. K$_2$O and Mg/(Mg + Fe^{2+}) versus SiOr values of 1-atm melts. (a) The K$_2$O content of melts along the plag + ol + aug, plag + ol + pig, plag + ol + opx, plag + aug + pig, and plag + aug + opx + mt LLMS are plotted against SiOr values, from the Plag + Mt projection. (b) Mg/(Mg + Fe^{2+}) values [*not* the Mg/(Mg + Fe$_{tot}$)] of melts plotted against SiOr values. The amount of Fe^{2+} was calculated using the method of Sack et al. (1980) at the same conditions of temperature and oxygen fugacity as used to construct the pseudoternary diagrams. "Walker"—data from Walker et al. (1979); "Grove"—data from Grove et al. (1982).

(1979) and Grove et al. (1982) are less potassic than the andesitic melts used in this study; their melts were in fact MORBs and an unusual high-alumina basalt anomalously low in K$_2$O (0.09 wt%) compared to typical high-alumina basalts (cf. Grove et al., 1982; Kuno, 1960). We attribute the differences in phase diagrams to these differences in K$_2$O.

Although a rationale of the different phase diagrams is not necessary to our arguments, we propose that the phase diagrams reflect different intersections of solidus surfaces with pyroxene phase relations. An analogy in a synthetic system is the demonstration by Kushiro (1969) in CaO-MgO-SiO$_2$-H$_2$O that the assemblage Fe-free pigeonite + diopside crystallizes at 20 kbar under anhydrous conditions but that orthopyroxene + diopside crystallizes under H$_2$O-saturated conditions. The difference lies in the

failure of the lower-temperature H$_2$O-saturated solidus surface to intersect the subsolidus pigeonite field because temperatures are below the reaction pigeonite = augite + orthopyroxene (Lindsley, 1980). By analogy, we propose that more potassic liquids, with lower liquidus temperatures, crystallize orthopyroxene. Higher potash contents, independent of temperature, may also affect low-Ca pyroxene compositions (cf. Kushiro, 1975).

Eight-kilobar liquid lines of descent. In comparison to 1 atm, fields of aug + plag and low-Ca pyroxene + plag have expanded at the expense of the ol + plag field (Fig. 4a); plag + aug stability remains virtually unchanged (Fig. 4b). Pigeonite is the stable low-Ca pyroxene at 8 kbar, presumably because of high Fe/Mg ratios of residual melts (cf. Fujii and Bougault, 1983).

Phase relations (Figs. 4a, 4b) were constructed from all three types of experiments—"melting," "crystallization," and "forced-saturation." At 8 kbar, residual melts of AT-1, AT-112, and AT-41 do not undergo SiO$_2$ enrichment, unlike residual melts at 1 atm (App. Table 1; Figs. 4a, 4b). Tie lines between coexisting crystals and melts (Fig. 5) indicate why no SiO$_2$ enrichment occurs: there is a thermal divide on the LLMS for plag + aug + pig and a pseudoternary eutectic for plag + ol + aug + pig. Modally, the lack of SiO$_2$ enrichment is reflected in lower proportions of olivine and higher proportions of clinopyroxenes in crystallizing assemblages.

The topology of the phase diagram (Fig. 4a) is consistent with the system olivine-diopside-silica under anhydrous conditions at 20 kbar (Kushiro, 1969). The LLMS (Figs. 4a, 4b) are, moreover, consistent with literature data provided that melt compositions are selected for which Mg/(Mg + Fe$_{tot}$) values are less than 0.55, like the melts in this study. Such data include melting of tholeiites (Thompson, 1974; Stolper, 1980) and an alkalic basalt
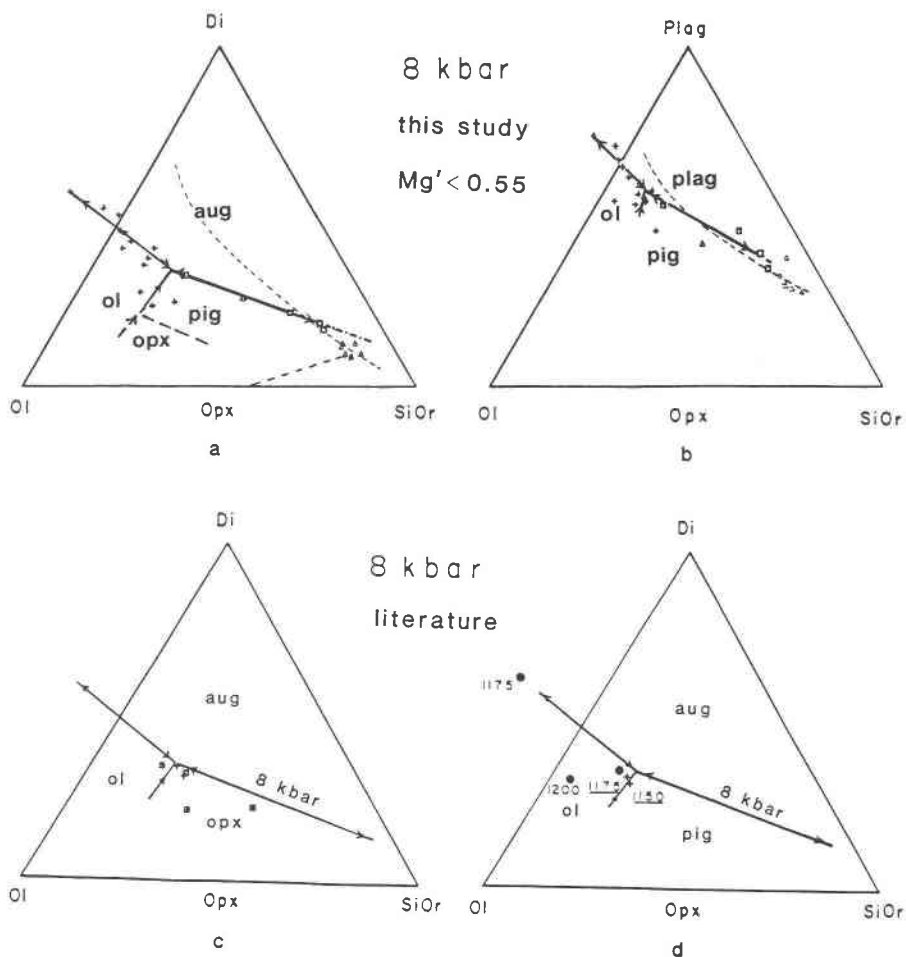
Fig. 4.   8-kbar pseudoternary diagrams. (a) Plag + Mt pseudoternary; (b) Di + Mt pseudoternary; +, (plag + ol + aug)– and (plag + ol + pig)–saturated melts; □, (plag + aug + pig)–saturated melts; △, (plag + pig)–saturated melts. Solid line, 8-kbar LLMSs (melt + plag + ol + pig, melt + plag + ol + aug, melt + plag + aug + pig); dashed line, 1-atm LLMSs (melt + plag + ol + aug, melt + plag + aug + opx + mt). (c) Compositions of high-Mg melts [Mg/(Mg + Fe$_{tot}$) > 0.55] coexisting with plag + ol + aug (+), plag + aug + opx (□), and plag + ol + aug + opx (cross within square) on (Plag + Mt)–saturated diagram. Analyses of melts from Bender et al. (1978), Stolper (1980), Fujii and Bougalt (1983), and Elthon and Scarfe (1984). The composition of glass coexisting with plag + ol + cpx (either augite or pigeonite) at 5 kbar from Takahashi and Kushiro (1983) is also plotted (■). (d) Compositions of low-Mg melts [Mg/(Mg + Fe$_{tot}$) < 0.55] coexisting with plag + ol + aug (+, 8-kbar melts; ●, 10-kbar melts) from Thompson (1974, 1975) and Stolper (1980) on (Plat + Mt)–saturated diagram. Numbers next to certain experiments are the temperatures at which the melt was produced; the nonunderlined numbers refer to the 10-kbar experiments, and the underlined numbers refer to the 8-kbar experiments. 8-kbar LLMS of this study are also plotted.

(Thompson, 1975) at 8–10 kbar (Fig. 4d). Thompson's (1974, 1975) experiments, when compositions are considered together with temperatures (plotted next to projected melt compositions; Fig. 4d), in fact also confirm the presence of two thermal divides.

On the other hand, the LLMS (Fig. 4a) are not consistent in phase assemblage with literature-derived melt compositions for which Mg/(Mg + Fe$_{tot}$) is greater than 0.55 and for which the low-Ca pyroxene is orthopyroxene, not pigeonite. Such experiments, largely on MORB compositions, typically did not involve plagioclase (e.g., Takahashi and Kushiro, 1983), but the few experiments at 7.5–10 kbar that did involve plagioclase (Fujii and

Bougault, 1983; Elthon and Scarfe, 1984; Bender et al., 1978) constrain Figure 4c. It may be noted that the pseudo-eutectics in Figures 4a and 4c, although involving different low-Ca pyroxenes, are at essentially the same position.

Compositions of H₂O-undersaturated melts

Limitations imposed by Fe loss. Because H₂O-CO₂ fluid compositions cannot be widely varied in graphite capsules, hydrous experiments were performed using noble-metal capsules and, despite all precautions (see above), samples lost Fe to capsules. Loss of Fe affects melt compositions in two ways. The first is the concentration effect
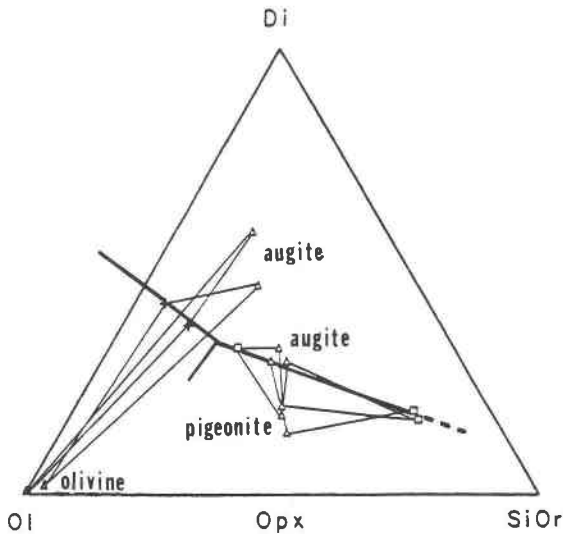
Fig. 5. Compositions of coexisting melts and mafic crystals at 8 kbar projected from Plag + Mt; +, (plag + ol + aug)–saturated melts; □, (plag + aug + pig)–saturated melts; △, coexisting augites and pigeonites or olivines and augites. Tielines connecting the phases indicate the presence of thermal divides on both the plag + ol + aug and plag + aug + pig liquid lines of multiple saturation.

that occurs in any multicomponent solution when one component is removed; the second is that increasing Mg/(Mg + Fe$_{tot}$) values lead to higher liquidus temperatures for ferromagnesian minerals, relative to plagioclase and other nonferromagnesian minerals, and therefore lead to different liquid lines of descent. Because of these effects, a liquid line of descent for a specific bulk composition with 2% H$_2$O in the melt cannot be determined.

Continuous Fe loss during experiments might be expected to result in disequilibrium compositions of melts and crystals; to investigate this possibility, partitioning of Fe and Mg between melts and crystals was investigated at NNO oxygen fugacity at both 1 atm and 2 kbar. This should be a reliable test of equilibrium as partitioning between olivine and melt is known to be relatively insensitive to pressure and temperature (Takahashi and Kushiro, 1983). In fact the 1-atm equilibrium, or at least steady-state, K_D values [(Fe$_{tot}$/Mg)$_{crystal}$ divided by (Fe$_{tot}$/Mg)$_{melt}$] and the 2-kbar K_D values compare favorably (Table 3) (except for experiments 1148 and 1174 which have much lower K_D values than observed in other experiments). All olivine K_D values are near the "ideal" 0.30 when melts are corrected for Fe^{3+} content by the method of Sack et al. (1980). On this basis, which is admittedly not perfect, most 2-kbar experiments appear to demonstrate equilibrium K_D values for olivine, augite, and orthopyroxene. The two experiments with low K_D values also have the highest Fe/Mg ratios of the melts; it is possible that high Fe/Mg ratios affect the partitioning of Fe and Mg between crystals and melt (cf. Mysen, 1982). The plag + aug + opx LLMS determined from 1148 and 1174

is consistent with plag + aug + opx LLMS of other 2-kbar experiments and was therefore used in constructing the pseudoternary diagrams.

Even though experiments may closely approach equilibrium, if Fe loss has created melts falling outside of the range of natural rock compositions, then application of the experimental results to igneous petrogenesis is highly questionable. To test the experimentally produced melts, Mg/(Mg + Fe$_{tot}$) and SiOr values of a suite of rocks from the Aleutian island of Atka were determined. Ratios of those values from the rocks were compared with the ratios determined for experimentally produced melts. Except for the only 5-kbar experiment containing olivine, all melts used to construct the hydrous pseudoternary diagrams have ratios of Mg/(Mg + Fe$_{tot}$) to SiOr similar to ratios of Atka rocks. Thus, despite Fe loss, the hydrous melts produced in this study are similar in composition to andesites found in intraoceanic island arcs.

Hydrous melt compositions projected onto pseudoternary diagrams. Baker and Eggler (1983) suggested that first-order effects of total pressure and H$_2$O pressure on 1-atm pseudoternaries are the following: (1) in Plag + Mt projection (Figs. 4a, 6a), pressure shifts the plag + ol + aug LLMS toward olivine composition, but H$_2$O content has little effect; pressure also shifts the plag + ol + low-Ca pyroxene LLMS toward olivine, but H$_2$O content shifts it away from olivine; (2) in the Ol + Mt projection, positions of the LLMS are functions of both pressure and H$_2$O content; however, in Di + Mt projections (Figs. 4b, 6b), H$_2$O content shifts the plag + aug + low-Ca pyroxene LLMS toward the plagioclase apex, owing to dramatic lowering of plagioclase liquidi relative to ferromagnesian mineral liquidi, whereas total pressure has a minor effect. Thus, to a first approximation, the Plag + Mt projection can be used as a geobarometer and the Di + Mt projection as a geohygrometer. Baker and Eggler (1983) based their predictions on synthetic systems (e.g., Kushiro, 1969), on existing natural hydrous systems (e.g., Eggler and Burnham, 1973), and on new experiments. Relatively meager amounts of data available in 1983 necessitated the use of olivine-saturated phase equilibria and therefore the pressure- and H$_2$O-sensitive Ol + Mt projection. Data of this study allow use of the superior, relatively pressure-insensitive, Di + Mt projection.

The new hydrous data at 2 kbar (Figs. 6a, 6b) completely follow the predictions of Baker and Eggler (1983). Compared to the 2-kbar results, a surprising element of the 5-kbar data is the expansion of the augite field; the expansion presumably can be attributed to pressure rather than to H$_2$O content. The experiments also demonstrate that orthopyroxene melts incongruently from 1 atm to at least 5 kbar and that no thermal divide exists to prevent production of andesitic melts from basaltic melts by crystallization fractionation (cf. Kushiro, 1969; Warner, 1973).

Other investigations. Investigations at crustal pressures of hydrous melting of basalts or of compositions of partial melts, or both, have been performed by Holloway
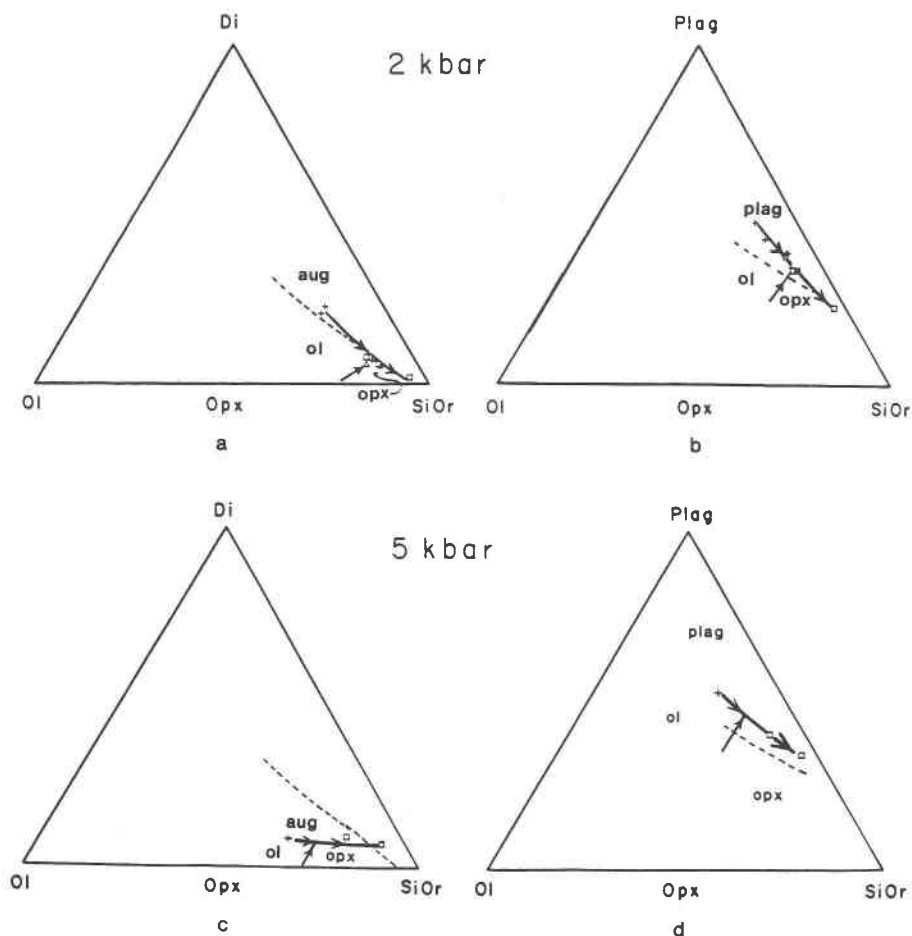
Fig. 6. H₂O-undersaturated melts (2% H₂O in *melt*) coexisting with plag + ol + aug (+) and plag + aug + opx (□). (a) 2-kbar Plag + Mt pseudoternary; (b) 2-kbar Di + Mt pseudoternary. △, composition of a melt coexisting with plag + aug + opx (optically identified only; no orthopyroxene was found with the probe. Solid line, 2-kbar LLMS. Dashed lines, 1-atm LLMS for reference. (c) 5-kbar Plag + Mt pseudoternary; (d) 5-kbar Diop + Mt pseudoternary. Solid line, 5-kbar LLMS. Dashed line, 1-atm LLMS.

and Burnham (1972), Helz (1976), Cawthorn (1976), and Spulber and Rutherford (1983). Typically these experiments contained large amounts of water (~4 to 8%) resulting in amphibole stability and consequent dramatic changes in liquid lines of descent. Only Spulber and Rutherford (1983) obtained analyses of hydrous basaltic to rhyolitic melts coexisting with plagioclase, olivine, and pyroxenes (augite and pigeonite, without orthopyroxene), but these phases were synthesized at much lower oxygen fugacities than in this study. Nevertheless, calculation of their 1–2-kbar melt compositions locates an LLMS for plag + ol + aug (with oxide phases) that agrees with the LLMS of this study. Andesite experiments in this study are comparable to studies by Eggler (1972), Eggler and Burnham (1973), Sekine et al. (1979), and Merzbacher and Eggler (1984), who located a family of LLMS for plag + opx + cpx and for H₂O contents between 0 and 4 wt%. Merzbacher and Eggler (1984) did not determine the type of clinopyroxene coexisting with the melts, but similarities between the melt compositions of Merzbacher and

Eggler (1984) and those of this study strongly support the assumption by Merzbacher and Eggler that the clinopyroxene was augite.

APPLICATION OF EXPERIMENTAL RESULTS TO PETROGENESIS OF ATKA HIGH-ALUMINA BASALTS AND ANDESITES

The possible petrogenetic link, through a process of crystallization fractionation, between high-alumina basalt and associated andesites has long been recognized (Bowen, 1928; Kuno, 1950; Osborn, 1959), although not accepted by all petrologists (e.g., Fenner, 1931; Mysen, 1982). The results of this investigation are consistent with the hypothesis that andesites, in particular Atka andesites, can be produced by crystallization fractionation from parental high-alumina basalts at crustal pressures.

Crystallization fractionation models

One atmosphere. On a Plag + Mt projection (Fig. 7a), basalt analyses do not fall along the LLMS for plag +
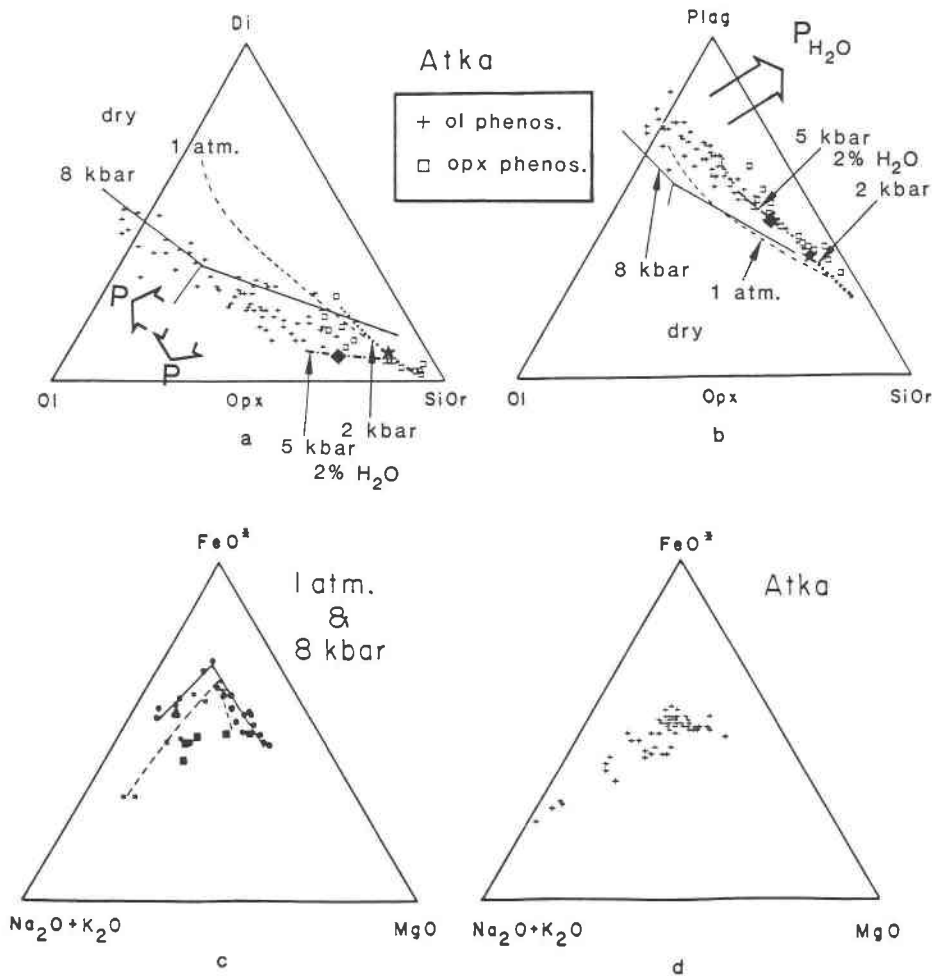
Fig. 7.   Comparison of experimental LLMS and compositions of rocks from the Aleutian island of Atka. (a) Plag + Mt pseudoternary; (b) Di + Mt pseudoternary. Large arrows on Plag + Mt pseudoternary indicate pressure effects on locations of the LLMS and the olivine–low-Ca pyroxene boundary point. Large arrow on Di + Mt pseudoternary indicates the effect of increasing H_2O pressure on the LLMS. Solid line, 8-kbar LLMS; dashed line, 1-atm LLMS; dotted line, 2-kbar LLMS; dash-dot line, 5-kbar LLMS; ⋆, olivine-orthopyroxene boundary point on the 2-kbar LLMS; ◆, olivine-orthopyroxene boundary point on the 5-kbar LLMS; +, compositions of rocks with phenocrystic olivine; □, compositions of rocks with phenocrystic orthopyroxene. (c) AFM diagram of bulk compositions of starting materials (filled squares) together with compositions of melts produced at 1 atm along the NNO buffer (the asterisks) and at 8 kbar (filled circles). (d) AFM plot of Atka rock compositions. Rock compositions courtesy of B. D. Marsh (pers. comm., 1980).

ol + aug, but some of the andesite analyses do plot along the LLMS for plag + aug + opx. On a Di + Mt projection, however, all natural rocks plot at much higher Plag values than the 1-atm LLMS. Furthermore, Fe enrichment of experimental melts (Fig. 7c) is greater than the "calc-alkaline" AFM trend of the Atka rock suite (Fig. 7d). Andesites of Atka could not be produced from dry high-alumina basalts by fractionation of plag + ol + aug at low pressure, nor could silica-rich andesites or dacites be produced from silica-poor andesites by fractionation of a plag + aug + opx + mt crystalline assemblage from anydrous melts at low pressure.

Eight kilobars. The 8-kbar LLMS (Figs. 7a, 7b) overlap Atka rock compositions in the Plag + Mt projection, but not in the Di + Mt projection. High-pressure fractionation of plag + ol + aug or plag + aug + pig, moreover,

cannot be responsible for generation of the complete Atka rock suite, because of the presence of a thermal divide on the plag + aug + pig LLMS and because, with crystallization, the 8-kbar melts become too impoverished in Al_2O_3 and too enriched in FeO* and TiO_2 relative to Atka rocks.

Two and five kilobars at H_2O-undersaturated conditions. The 2- and 5-kbar LLMS either coincide with or bracket basaltic andesite to dacitic rock compositions of the Atka suite on both Plag + Mt projections and Di + Mt projections (Figs. 7a, 7b). Therefore andesite melts can fractionate from evolved high-alumina basalts or basaltic andesites (similar in composition to AT-41) by the crystallization of plag + ol + aug between 2 and 5 kbar for H_2O contents of about 2 wt% (in the resulting andesitic melts). Those pressure estimates are also compatible

with the relative positions of Atka olivine-bearing versus orthopyroxene-bearing andesites (Fig. 7a). Presumably, H_2O content of parental basaltic or basaltic andesite magmas was near 1 wt%. Andesitic melts can produce dacitic residual melts by the fractionation of plag + aug + opx at the same conditions of pressure and similar, but slightly higher, H_2O contents.

A petrologically favorable consequence of slightly hydrous fractionation is that proportions of plagioclase in crystallizing assemblages are reduced (App. Table 1) with concomitant increases in proportions of augite. Increase in modal augite is important in production of residual melts that are not strongly enriched in TiO_2, because augite is the only crystal in these experiments that is a suitable host for Ti.

Although basaltic andesites of Atka can be linked to andesites and dacites of Atka through crystallization fractionation at crustal pressures with approximately 2% H_2O in the melt, a mechanism linking more primitive high-alumina basalts (e.g., AT-1 and AT-112) to basaltic andesites (AT-41) is equivocal because of the lack of direct experimental data on the hydrous plag + aug + ol LLMS for melts with composition similar to the more primitive high-alumina basalts. It should be noted, however, that extrapolation of the hydrous 2- and 5-kbar plag + ol + aug LLMS to more basaltic compositions is on trend with Atka basalts in the Di + Mt projection (Fig. 7b), suggesting the hydrous nature of Atka basalts. In Plag + Mt projection (Fig. 7a), the array of Atka basalts suggests fractionation at pressures near 5 to 8 kbar.

The H_2O content of Atka andesitic and dacitic melts is unlikely to have been much higher than 2 wt%. Merzbacher and Eggler (1984) clearly demonstrated the sensitivity of the plag + aug + opx LLMS to water content when displayed on a diopside-saturated projection and developed a geohygrometer for use on andesitic to dacitic melts. On the basis of their research, the plag + aug + opx LLMS with 4 wt% H_2O would plot at higher Plag values than observed for the dacitic portion of the Atka rock suite.

Hydrous experimental results have not defined the role of magnetite in the generation of Atka andesite with magnetite. Magnetite was absent in hydrous experiments because of relatively low oxygen fugacities (Baker and Eggler, 1983; Baker, 1985). Magnetite is required for many crystallization fractionation calculations (e.g., Gill, 1981) and is present in Atka rocks, but in both cases magnetite only occurs in small amounts; such small amounts of magnetite are not inconsistent with the conclusions of this study which stress the importance of crystallization fractionation of plag + ol + aug or plag + aug + opx in the petrogenesis of Atka rocks.

Depth of magma chambers beneath the Aleutian island of Atka

As argued above, comparison of Atka rocks and experimental LLMS on pseudoternary diagrams indicates that Atka andesites evolved in magma chambers at the relatively shallow depths of 7 to 17 km (2–5 kbar). Evolution of basaltic andesites also probably occurred in chambers at similar depths. Basalts, however, may have evolved in deeper magma chambers at ~26 km (8 kbar; see above). In addition to that relatively deep history, basalts also record residence in more shallow magma chambers for a time period sufficient to dissolve any clinopyroxene phenocrysts originally present in the more primitive members of the suite (Baker and Eggler, 1983). Therefore, at least two levels of magma chambers exist beneath Atka. Primitive high-alumina basaltic magmas, produced by partial melting, appear to undergo limited fractionation at ~26 km; they then ascend to crustal magma chambers (7–17 km) where the melts evolve to more silica-rich high-alumina basalts, basaltic andesites, andesites, and dacites. Magmas then probably rise into a third level of subvolcanic magma chambers that are tapped during eruption.

CONCLUSIONS

Anhydrous experiments indicate the lack of a 1-atm phase field of pigeonite for andesitic and basaltic compositions studied, whereas such a pigeonite field exists at 8 kbar. The lack of the pigeonite stability field precludes the existence of a low-pressure thermal divide for the compositions studied along a LLMS where olivine coexists with pigeonite. At 1 atm, andesites exhibit a reaction point where olivine reacts with the melt, and orthopyroxene and magnetite begin to crystallize. At 8 kbar, a thermal divide exists along both the plag + aug + ol and the plag + aug + pig LLMS; these thermal divides prevent the formation of alkali basalts from tholeiites and the production of andesites from basalts under anhydrous conditions and deep-crustal pressures.

At 2 and 5 kbar, with 2% H_2O in the melt, orthopyroxene is the observed low-Ca pyroxene, and no thermal divides exist on the LLMS; under these conditions of pressure and H_2O content, basaltic and andesitic magmas can evolve toward silica enrichment through the crystallization fractionation of plagioclase, augite, and either olivine or orthopyroxene.

Comparisons of LLMS and Atka rock compositions on suitable pseudoternary projections suggest that andesitic members of the suite evolved in magma chambers at pressures between 2 and 5 kbar from magmas of basaltic andesite composition. H_2O contents of 2 wt% are estimated for Atka andesites. Evolution of Atka high-alumina basalts occurred in deeper magma chambers, at 5–8-kbar pressure.

REFERENCES

Albee, A.L., and Ray, R. (1970) Correction factors for electron probe microanalysis of silicates, oxides, carbonates, phosphates and sulphates. Analytical Chemistry, 42, 1408–1414.

Allen, J.C., and Boettcher, A.L. (1978) Amphiboles in andesite and basalt: II. Stability as a function of P-T-fH_2O-fO_2. American Mineralogist, 63, 1074–1087.

Allen, J.C., Boettcher, A.L., and Marland, G. (1975) Amphiboles in andesite and basalt: I. Stability as a function of P-T-fO_2. American Mineralogist, 60, 1069–1085.

Baker, D.R. (1985) The compositions of melts coexisting with plagioclase, olivine, augite, orthopyroxene, and pigeonite at pressures from one atmosphere to 20 kbar and application to petrogenesis in intraoceanic island arcs. Ph.D. thesis, Pennsylvania State University, University Park.

Baker, D.R., and Eggler, D.H. (1983) Fractionation paths of Atka (Aleutians) high-alumina basalts: Constraints from phase relations. Journal of Volcanology and Geothermal Research, 18, 387–404.

Bence, A.E., and Albee, A.L. (1968) Empirical correction factors for the electron microanalysis of silicates and oxides. Journal of Geology, 76, 382–403.

Bender, J.F., Hodges, F.N., and Bence, A.E. (1978) Petrogenesis of basalts from the Project FAMOUS area: Experimental study from 0 to 15 kbars. Earth and Planetary Science Letters, 41, 277–302.

Bohlen, S.R., Boettcher, A.L., Wall, V.J., and Clemens, J.D. (1983) Stability of phlogopite-quartz and sanidine-quartz: A model for melting in the lower crust. Contributions to Mineralogy and Petrology, 83, 270–277.

Bowen, N.L. (1928) The evolution of the igneous rocks. Princeton University Press, Princeton, N.J.

Boyd, F.R., and England, J.L. (1960) Apparatus for phase-equilibrium measurements at pressures up to 50 kilobars and temperatures up to 1750°C. Journal of Geophysical Research, 65, 741–748.

Bryan, W.B., Finger, L.W., and Chayes, F. (1969) A least-squares approximation for estimating the composition of a mixture. Carnegie Institution of Washington Yearbook, 67, 243–244.

Burnham, C.W. (1979) The importance of volatile constituents. In H.S. Yoder, Ed. The evolution of igneous rocks, fiftieth anniversary perspectives, p. 439–482. Princeton University Press, Princeton.

——— (1981) The nature of multicomponent aluminosilicate melts. In D.T. Rickard and F.E. Wickman, Eds. Chemistry and geochemistry at high temperatures and pressures, p. 197–229. Pergammon Press, New York.

Cawthorn, R.G. (1976) Melting relations in part of the system CaO-MgO-Al$_2$O$_3$-SiO$_2$-Na$_2$O-H$_2$O under 5 kb pressure. Journal of Petrology, 17, 44–72.

Cawthorn, R.G., Curran, E.B., and Arculus, R.J. (1973) A petrogenetic model for the origin of the calc-alkaline suite of Grenada, Lesser Antilles. Journal of Petrology, 14, 327–337.

Coulon, C., and Thorpe, R.S. (1981) Role of continental crust in petrogensis of orogenic volcanic associations. Tectonophysics, 77, 79–94.

Dixon, T.H., and Batiza, R. (1979) Petrology and chemistry of recent lavas in the Northern Marianas: Implications for the origin of island arc basalts. Contributions to Mineralogy and Petrology, 70, 167–181.

Dixon, T.H., and Stern, R.J. (1983) Petrology, chemistry and isotopic composition of submarine volcanoes in southern Mariana arc. Geological Society of America Bulletin, 94, 1159–1172.

Eggler, D.H. (1972) Water-saturated and undersaturated melting relations in a Paracutin andesite and an estimate of water content in the natural magma. Contributions to Mineralogy and Petrology, 34, 261–271.

Eggler, D.H., and Burnham, C.W. (1973) Crystallization and fractionation trends in the system andesite-CO$_2$-H$_2$O at pressures to 10 kb. Geological Society of America Bulletin, 84, 2517–2532.

Eggler, D.H., and Osborn, E.F. (1982) Experimental studies of the system MgO-FeO-Fe$_2$O$_3$-NaAlSi$_3$O$_8$-CaAl$_2$Si$_2$O$_8$-SiO$_2$ — A model for subalkaline magmas. American Journal of Science, 282, 1012–1041.

Eichelberger, J.C. (1975) Origin of andesite and dacite: Evidence of mixing at Glass Mountain in California and at other circum-Pacific volcanoes. Geological Society of America Bulletin, 86, 1381–1391.

Elthon, D., and Scarfe, C.M. (1984) High-pressure phase equilibria of a high-magnesia basalt and the genesis of primary oceanic basalts. American Mineralogist, 69, 1–15.

Ewart, A. (1982) The mineralogy and petrology of Tertiary-Recent orogenic volcanic rocks, with special reference to the andesitic-basaltic compositional range. In R.S. Thorpe, Ed. Andesites: Orogenic andesites and related rocks, p. 25–95. Wiley, New York.

Fenner, C.N. (1931) The residual liquids of crystallizing magmas. Mineralogical Magazine, 22, 539–560.

Fujii, T., and Bougault, H. (1983) Melting relations of a magnesian abyssal tholeiite and origin of MORB's. Earth and Planetary Science Letters, 62, 285–295.

Gibb, F.G.F. (1974) Supercooling and the crystallization of plagioclase from a basaltic magma. Mineralogical Magazine, 39, 641–653.

Gill, J. (1981) Orogenic andesites and plate tectonics. Springer-Verlag, New York.

Green, T.H., and Ringwood, A.E. (1968) Genesis of the calc-alkaline igneous rock suite. Contributions to Mineralogy and Petrology, 18, 105–162.

Grove, T.L., and Bryan, W.B. (1983) Fractionation of pyroxene-phyric MORB at low pressure: An experimental study. Contributions to Mineralogy and Petrology, 84, 293–309.

Grove, T.L., Gerlach, D.C., and Sando, T.W. (1982) Origin of calc-alkaline series lavas at Medicine Lake Volcano by fractionation, assimilation and mixing. Contributions to Mineralogy and Petrology, 80, 160–182.

Helz, R.T. (1976) Phase relations of basalts in their melting ranges at P H$_2$O = 5 kb. Part II. Melt compositions. Journal of Petrology, 17, 139–193.

——— (1978) The petrogenesis of the Ice Harbor Member, Columbia River Plateau, Washington: A chemical and experimental study. Ph.D. thesis, Pennsylvania State University, University Park.

Holloway, J.R. (1971) Internally heated pressure vessels. In G.C. Ulmer, Ed. Research techniques for high pressures and high temperatures, p. 217–258. Springer-Verlag, New York.

——— (1976) Fluids in the evolution of granitic magmas: Consequences of finite CO$_2$ solubility. Geological Society of America Bulletin, 87, 1513–1518.

——— (1977) Fugacity and activity of molecular species in supercritical fluids. In D.G. Fraser, Ed. Thermodynamics in geology, p. 161–180. D. Reidel, Dortrecht.

Holloway, J.R., and Burnham, C.W. (1972) Melting relations of basalt with equilibrium water pressure less than total pressure. Journal of Petrology, 13, 1–29.

Irvine, T.N. (1974) Petrology of the Duke Island ultramafic complex, southeastern Alaska. Geological Society of America Memoir 138, 240 p.

Kay, S.M., Kay, R.W., and Citron, G.P. (1982) Tectonic controls on tholeiitic and calcalkaline magmatism in the Aleutian arc. Journal of Geophysical Research, 87, 4051–4072.

Kuno, H. (1950) Petrology of Hakone Volcano and the adjacent areas, Japan. Geological Society of America Bulletin, 61, 957–1020.

——— (1960) High alumina basalt. Journal of Petrology, 1, 121–145.

Kushiro, I. (1969) The system forsterite-diopside-silica, with and

without water at high pressures. American Journal of Science, 267A, 269–294.

——— (1975) On the nature of silicate melt and its significance in magma genesis: Regularities in the shift of the liquidus boundaries involving olivine, pyroxene, and silica minerals. American Journal of Science, 275, 411–432.

Leeman, W.P. (1983) The influence of crustal structure on compositions of subduction-related magmas. Journal of Volcanological and Geothermal Research, 18, 561–588.

Lindsley, D.H. (1980) Phase equilibria at pressures > 1 atmosphere. Mineralogical Society of America Reviews in Mineralogy, 7, 289–308.

Mahood, G.A., and Baker, D.R. (1986) Experimental constraints on depths of fractionation of mildly alkalic basalts and associated felsic rocks: Pantelleria, Strait of Sicily. Contributions to Mineralogy and Petrology, 93, 251–264.

Marsh, B.D. (1982) The Aleutians, In R.S. Thorpe, Ed. Andesites: Orogenic andesites and related rocks, p. 99–113. Wiley, New York.

Merzbacher, C.I., and Eggler, D.H. (1984) A magmatic geohygrometer: Application to Mount St. Helens and other dacitic magmas. Geology, 12, 587–590.

Mysen, B.O. (1982) The role of mantle anatexis. In R.S. Thorpe, Ed. Andesites: Orogenic andesites and related rocks, p. 489–522. Wiley, New York.

O'Hara, M.J. (1968) The bearing of phase equilibria studies in synthetic and natural systems on the origin and evolution of basic and ultrabasic rocks. Earth Science Reviews, 4, 69–133.

Osborn, E.F. (1959) The role of oxygen pressure in the crystallization and differentiation of basaltic magma. American Journal of Science, 257, 609–647.

——— (1979) The reaction principle. In H.S. Yoder, Ed. The Evolution of the igneous rocks, fiftieth anniversary perspectives, p. 133–170. Princeton University Press, Princeton, N.J.

Sack, R.O., Carmichael, I.S.E., Rivers, M., and Ghiorso, M.S.

(1980) Ferric-ferrous equilibria in natural silicate liquids at 1 bar. Contributions to Mineralogy and Petrology, 75, 369–376.

Sekine, T., Katsura, T., and Aramaki, S. (1979) Water saturated phase relations of some andesites with application to the estimation of the initial temperature and water pressure at the time of eruption. Geochimica et Cosmochimica Acta, 43, 1367–1376.

Spulber, S.D., and Rutherford, M.J. (1983) The origin of rhyolite and plagiogranite in oceanic crust: An experimental study. Journal of Petrology, 24, 1–25.

Stern, R.J. (1979) On the origin of andesite in the Northern Mariana island arc: Implications from Agrigan. Contributions to Mineralogy and Petrology, 68, 207–219.

Stolper, E. (1980) A phase diagram for mid-ocean ridge basalts: Preliminary results and implications for petrogenesis. Contributions to Mineralogy and Petrology, 74, 13–27.

Takahashi, E., and Kushiro, I. (1983) Melting of a dry peridotite at high pressures and basalt magma genesis. American Mineralogist, 68, 859–879.

Thompson, R.N. (1974) Primary basalts and magma genesis, I. Skye, north-west Scotland. Contributions to Mineralogy and Petrology, 45, 317–341.

——— (1975) Primary basalts and magma genesis. II. Snake River plain, Idaho, U.S.A. Contributions to Mineralogy and Petrology, 52, 213–232.

Walker, D., Shibata, T., and DeLong, S.E. (1979) Abyssal tholeiites from the Oceanographer fracture zone. II. Phase equilibria and mixing. Contributions to Mineralogy and Petrology, 70, 111–125.

Warner, R.D. (1973) Liquidus relations in the system CaO-MgO-SiO₂-H₂O at 10 kb P H₂O and their petrologic significance. American Journal of Science, 273, 925–946.

Appendix Table 1. Experimental conditions, results, and analyses

Run (hrs.)	Temp. °C (log fO2)	Phase (mode)	n	SiO₂	TiO₂	Al₂O₃	FeO*	MnO	MgO	CaO	Na₂O	K₂O	P₂O₅	Total
							1 atm Experiments							
		Starting Composition:	AT-112											
1304	1122	Glass(34)	7	51.4(4)	2.12(18)	13.0(4)	13.5(4)	0.39(5)	4.55(20)	9.50(3)	2.65(12)	1.23(8)	0.35(4)	98.69
(96)	(-8.5)	Plag(49)	6	52.3(9)	0.0	29.2(4)	1.31(12)	0.0	0.15(7)	13.5(3)	3.45(12)	0.23(2)	0.0	100.14
		Oliv(12)	4	38.0(4)	0.0	0.22(2)	26.4(3)	0.56(9)	33.5(6)	0.63(5)	0.0	0.0	0.0	99.31
		Aug(4)	6	51.3(5)	0.51(12)	2.37(26)	10.3(53)	0.36(9)	14.3(8)	20.1(3)	0.13(4)	0.0	0.0	99.37
1280	1100	Glass(13)	5	52.3(7)	3.27(17)	12.3(3)	13.7(5)	0.34(4)	3.83(13)	8.61(21)	2.15(18)	1.46(8)	0.46(8)	98.42
(192)	(-8.8)	Plag(62)	5	55.2(9)	0.0	28.0(7)	1.04(6)	0.0	0.09(4)	12.0(5)	4.32(57)	0.41(4)	0.0	101.06
		Oliv(16)	4	37.2(3)	0.05(5)	0.29(10)	31.6(2)	0.71(7)	29.7(3)	0.63(2)	0.0	0.0	0.0	100.18
		Aug(10)	4	51.2(6)	0.92(16)	1.95(25)	11.9(5)	0.54(5)	14.3(3)	19.1(3)	0.22(13)	0.0	0.0	100.13
		Starting Composition:	AT-29											
1086	1106	Glass(69)	5	59.2(1)	1.23(13)	14.6(2)	8.61(5)	0.22(7)	2.74(9)	5.82(16)	3.70(23)	2.75(5)	0.32(5)	99.19
(192)	(-8.7)	Plag(26)	5	55.7(3)	0.0	27.2(6)	0.91(2)	0.0	0.14(8)	11.2(2)	4.76(27)	0.53(7)	0.0	100.44
		Oliv(5)	5	37.1(2)	0.15(12)	0.19(3)	30.6(1)	0.76(4)	30.7(1)	0.50(1)	0.0	0.0	0.0	100.00
		Aug(1)	5	51.8(5)	0.43(7)	1.76(3)	11.3(5)	0.58(7)	14.6(3)	18.4(5)	0.27(10)	0.0	0.0	99.14
3	1095	Glass(51)	5	63.7(6)	1.14(9)	14.3(3)	7.36(19)	0.0	1.61(15)	3.78(38)	4.21(27)	4.22(25)	0.33(14)	100.65
(195)	(-8.9)	Plag(34)	5	56.7(2)	0.09(6)	28.3(4)	0.99(11)	0.0	0.16(4)	10.6(5)	5.38(15)	0.70(12)	0.0	102.92
		Aug(8)	5	52.2(9)	0.53(9)	1.67(26)	11.2(1)	0.0	15.5(5)	19.0(5)	0.42(5)	0.0	0.0	100.52
		Opx(4)	5	52.4(9)	0.30(5)	0.85(9)	20.5(4)	0.0	23.7(7)	2.02(15)	0.06(2)	0.0	0.0	99.87
		Opaq(3)	5	0.39(6)	11.5(6)	3.50(22)	77.4(3)	0.0	3.40(18)	0.20(4)	0.0	0.0	0.0	96.39
874	1083	Glass(47)	6	65.8(2)	1.16(15)	14.9(6)	4.31(1)	0.13(3)	1.72(9)	3.64(26)	3.76(24)	3.99(15)	0.53(6)	99.94
(192)	(-9.0)	Plag(36)	5	55.3(5)	0.0	27.2(7)	0.95(9)	0.0	0.03(2)	11.0(6)	4.76(14)	0.53(7)	0.0	99.77
		Aug(8)	5	51.8(5)	0.55(14)	2.03(3)	10.8(5)	0.58(4)	14.4(2)	19.2(4)	0.26(5)	0.0	0.0	99.62
		Opx(3)	4	54.1(2)	0.32(11)	1.09(14)	14.9(5)	0.90(4)	26.2(3)	2.16(2)	0.0	0.0	0.0	99.67
		Opaq(6)	4	0.76(7)	4.92(19)	3.69(16)	76.4(8)	0.84(9)	5.74(30)	0.21(5)	0.0	0.0	0.0	92.56
11	1060	Glass(37)	2	66.2(14)	0.70(2)	14.7(3)	4.94(28)	0.0	0.78(9)	1.98(4)	3.71(26)	5.19(22)	0.26(3)	98.46
(480)	(-9.4)	Plag(42)	4	57.4(9)	0.0	26.4(6)	0.93(15)	0.0	0.08(3)	9.43(16)	5.81(22)	0.67(12)	0.0	100.72
		Aug(12)	8	51.5(10)	0.52(5)	1.98(29)	11.2(3)	0.0	14.5(4)	19.3(5)	0.33(5)	0.0	0.0	99.33
		Opx(5)	4	52.9(6)	0.29(2)	0.77(24)	20.7(3)	0.0	22.0(6)	1.87(8)	0.05(1)	0.0	0.0	98.58
		Opaq(5)	4	0.20(11)	15.3(8)	2.56(37)	73.6(3)	0.0	2.32(10)	0.20(3)	0.0	0.0	0.0	94.18
14	1060	Glass	2	66.8(8)	0.76(8)	14.4(9)	4.95(65)	0.0	0.80(9)	2.12(24)	3.11(46)	5.11(40)	0.31(29)	98.36
(24)	(-9.4)													
		Starting Composition:	AT-25											
1222	1100	Glass(68)	5	59.3(7)	1.22(6)	14.7(2)	8.13(43)	0.11(5)	2.43(5)	5.53(14)	3.56(20)	3.36(5)	0.33(3)	98.67
(192)	(-8.8)	Plag(26)	5	54.9(7)	0.0	27.5(3)	0.80(16)	0.0	0.08(7)	10.9(3)	4.69(23)	0.65(4)	0.0	99.52
		Oliv(4)	3	37.6(1)	0.14(4)	0.20(2)	28.1(1)	0.53(9)	32.5(7)	0.51(1)	0.0	0.0	0.0	99.58
		Aug(5)	5	51.3(5)	0.49(12)	1.67(14)	10.5(4)	0.46(7)	14.3(5)	19.9(3)	0.35(12)	0.0	0.0	98.97
4	1095	Glass(44)	6	63.6(9)	1.09(8)	14.6(4)	5.81(43)	0.0	1.42(11)	3.04(13)	4.00(11)	5.11(21)	0.34(8)	99.01
(195)	(-8.9)	Plag(38)	5	56.0(9)	0.0	26.9(7)	0.64(6)	0.0	0.07(2)	9.57(20)	5.51(29)	0.91(13)	0.0	99.60
		Aug(10)	3	51.1(3)	0.49(3)	1.70(13)	9.97(65)	0.0	14.6(3)	20.0(3)	0.43(7)	0.10(4)	0.0	98.39
		Opx(5)	3	51.7(1)	0.25(1)	0.89(42)	19.4(9)	0.0	23.6(7)	1.83(9)	0.07(3)	0.11(3)	0.0	97.85
		Opaq(3)	4	0.26(10)	11.3(5)	3.50(24)	74.3(7)	0.0	3.53(26)	0.17(6)	0.0	0.0	0.0	93.06

Appendix Table 1. *Continued*

Run (hrs.)	Temp. °C (log fO2)	Phase (mode)	n	SiO2	TiO2	Al2O3	FeO*	MnO	MgO	CaO	Na2O	K2O	P2O5	Total
886	1083	Glass(49)	5	64.2(5)	1.23(7)	14.9(8)	4.27(27)	0.21(6)	1.40(8)	3.61(31)	3.64(22)	4.48(7)	0.47(5)	98.41
(192)	(-9.0)	Plag(35)	4	56.0(9)	0.0	27.5(3)	0.64(8)	0.0	0.02(2)	10.7(3)	4.83(17)	0.72(3)	0.0	100.41
		Aug(7)	6	51.8(4)	0.52(20)	1.90(48)	10.1(6)	0.49(13)	14.2(8)	20.1(6)	0.40(14)	0.21(7)	0.0	99.51
		Opx(5)	4	54.2(9)	0.36(16)	1.30(14)	14.5(5)	0.74(17)	25.9(7)	2.16(21)	0.21(7)	0.0	0.0	99.37
		Opaq(4)	4	0.69(13)	5.54(51)	3.92(7)	75.4(5)	0.71(8)	5.51(28)	0.17(4)	0.0	0.0	0.0	91.94

8 kbar Experiments

Starting Composition: AT-1

Run (hrs.)	Temp. °C	Phase (mode)	n	SiO2	TiO2	Al2O3	FeO*	MnO	MgO	CaO	Na2O	K2O	P2O5	Total
934	1300/	Glass(60)	7	49.1(6)	1.62(16)	16.2(3)	13.5(7)	0.25(6)	6.13(19)	8.38(20)	3.22(18)	0.96(6)	0.23(4)	99.59
(1/24)	1175	Plag(35)	7	54.0(5)	0.0	28.5(2)	0.62(6)	0.0	0.10(4)	12.0(3)	4.22(19)	0.34(5)	0.0	99.78
		Oliv(4)	1	37.2	0.0	0.0	26.0	0.53	35.7	0.34	0.0	0.0	0.0	99.79
		Pig(4)	4	51.2(3)	0.64(7)	5.53(33)	14.8(2)	0.46(6)	21.5(5)	5.66(35)	0.18(3)	0.0	0.0	99.87
891	1150	Glass(38)	8	47.8(4)	2.62(24)	14.0(2)	16.2(3)	0.32(5)	4.67(8)	7.85(11)	3.32(13)	1.50(7)	0.53(7)	98.81
(24)		Plag(48)	4	55.8(6)	0.0	27.3(3)	0.76(42)	0.0	0.17(7)	11.0(6)	4.87(29)	0.56(6)	0.0	100.46
		Oliv(5)	6	36.5(4)	0.10(1)	0.03(3)	33.4(8)	0.57(8)	29.6(5)	0.4(6)	0.0	0.0	0.0	100.60
		Pig(9)	5	51.3(11)	0.53(9)	3.75(69)	17.1(5)	0.53(3)	20.2(6)	5.98(47)	0.13(3)	0.0	0.0	99.52
953	1300/	Glass(44)	6	47.6(4)	2.07(28)	14.9(2)	15.7(3)	0.31(4)	5.70(9)	8.23(7)	3.02(14)	1.16(3)	0.48(5)	99.17
(1/24)	1150	Plag(46)	5	54.0(3)	0.15(11)	27.9(22)	0.38(8)	0.03(2)	0.07(3)	11.9(2)	4.50(18)	0.40(4)	0.0	99.33
		Oliv(3)	2	37.3(3)	0.16(4)	0.0	32.0(4)	0.54(1)	32.0(2)	0.43(8)	0.0	0.0	0.0	100.43
		Pig(7)	5	51.9(4)	0.50(7)	4.57(56)	16.8(4)	0.46(5)	20.9(4)	5.80(35)	0.18(5)	0.0	0.0	101.11

Starting Composition: AT-41

1008	1125	Glass(41)	6	49.8(6)	3.06(17)	12.5(2)	17.1(5)	0.38(5)	3.09(29)	6.97(12)	3.11(20)	1.85(18)	0.70(9)	98.56
(96)		Plag(52)	6	59.6(8)	0.0	24.8(3)	0.69(10)	0.0	0.12(6)	8.35(26)	6.04(18)	0.95(4)	0.0	100.55
		Pig(7)	5	52.0(7)	0.61(24)	2.24(56)	24.0(7)	0.78(11)	16.9(5)	4.94(75)	0.16(6)	0.0	0.0	101.63

Starting Composition: AT-112

940	1175	Glass(59)	6	48.3(4)	1.20(16)	14.9(8)	13.9(9)	0.36(8)	7.45(37)	9.23(13)	2.33(31)	1.02(5)	0.25(3)	98.94
(24)		Plag(34)	4	51.9(3)	0.07(2)	29.5(3)	0.47(5)	0.02(1)	0.19(6)	13.4(15)	3.44(6)	0.28(1)	0.0	99.27
		Oliv(1)	4	39.0(4)	0.15(5)	0.07(3)	22.7(7)	0.39(5)	38.4(3)	0.36(4)	0.0	0.0	0.0	101.07
		Aug(6)	4	52.0(6)	0.67(13)	5.18(8)	10.7(6)	0.33(4)	18.9(6)	11.8(3)	0.06(7)	0.0	0.0	99.64
1098	1300/	Glass(6)	5	42.8(8)	5.63(31)	12.2(7)	20.0(9)	0.35(8)	3.63(29)	8.20(36)	2.27(17)	2.06(17)	1.55(23)	98.69
(1/24)	1175	Plag(60)	4	52.4(3)	0.0	29.7(4)	0.63(14)	0.0	0.13(3)	13.7(13)	3.69(16)	0.56(11)	0.0	100.79
		Oliv(11)	4	35.4(2)	0.10(6)	0.09(5)	40.5(10)	0.66(10)	24.1(4)	0.55(4)	0.0	0.0	0.0	101.40
		Aug(22)	4	48.8(6)	1.96(18)	6.50(7)	15.1(7)	0.37(5)	12.9(6)	14.7(11)	0.57(19)	0.0	0.0	100.90

Starting Composition: AT-29

1010	1125	Glass(43)	6	57.2(4)	1.65(16)	13.8(5)	10.9(2)	0.23(8)	2.23(7)	5.67(24)	3.78(17)	3.02(12)	0.40(3)	98.98
(96)		Plag(41)	4	58.0(5)	0.0	25.1(5)	0.54(16)	0.0	0.07(4)	8.54(11)	5.89(17)	1.18(6)	0.0	99.32
		Aug(4)	1	50.9	0.98	2.35	17.9	0.45	15.8	11.3	0.24	0.0	0.0	99.92
		Pig(12)	5	52.1(7)	0.30(9)	2.06(44)	19.0(6)	0.55(3)	19.2(15)	6.61(62)	0.15(4)	0.0	0.0	99.97
989	1300/	Glass(43)	7	56.4(7)	1.96(7)	13.4(2)	11.8(6)	0.31(5)	2.07(12)	5.76(14)	3.25(15)	3.29(13)	0.54(6)	98.78
(1/24)	1125	Plag(41)	5	58.7(4)	0.0	25.1(2)	0.36(5)	0.0	0.04(2)	8.55(16)	5.81(6)	1.40(17)	0.0	99.96
		Aug(1)	2	49.6(5)	0.71(8)	3.63(36)	18.3(5)	0.65(4)	15.3(1)	11.1(4)	0.33(6)	0.0	0.0	99.62
		Pig(14)	4	50.8(7)	0.65(8)	2.81(40)	20.7(7)	0.70(12)	16.7(3)	7.93(48)	0.22(6)	0.0	0.0	100.51

Starting Composition: AG7-1

910	1125	Glass(74)	6	61.0(5)	1.19(7)	13.4(3)	10.1(4)	0.25(6)	2.24(12)	4.99(11)	3.63(9)	2.34(8)	0.44(3)	99.58
(96)		Plag(23)	6	59.4(3)	0.13(7)	24.7(4)	0.38(4)	0.0	0.0	7.84(25)	6.09(21)	0.74(6)	0.0	99.28
		Pig(3)	1	52.1	0.42	1.71	23.2	0.82	18.5	4.17	0.0	0	0.0	100.89
917	1100	Glass(51)	7	61.7(5)	1.45(13)	12.5(3)	10.2(3)	0.30(6)	1.09(11)	4.23(7)	3.72(8)	2.93(5)	0.64(10)	98.76
(192)		Plag(38)	5	60.8(5)	0.16(6)	23.9(4)	0.62(8)	0.0	0.03(3)	6.75(37)	6.64(15)	1.10(8)	0.0	100.00
		Pig(11)	5	50.9(7)	0.46(2)	1.31(30)	25.1(6)	1.03(17)	16.5(4)	4.45(32)	0.02(3)	0.0	0.0	99.77
944	1175/	Glass(69)	8	60.8(7)	1.20(21)	13.2(3)	10.1(6)	0.28(5)	2.02(23)	4.81(22)	3.50(15)	2.42(13)	0.53(6)	98.86
(24/	1100	Plag(26)	7	59.9(7)	0.0	24.5(5)	0.43(5)	0.0	0.0	7.58(33)	6.31(9)	0.83(7)	0.0	99.55
96)		Pig(4)	6	51.3(4)	0.43(10)	1.56(8)	23.3(5)	0.72(10)	17.5(4)	4.53(28)	0.06(5)	0.0	0.0	99.60
1075	1075	Glass(73)	6	60.8(7)	0.89(21)	13.4(3)	10.2(5)	0.41(7)	2.14(7)	4.96(16)	3.98(20)	2.34(5)	0.46(4)	99.58
(192)		Plag(23)	7	59.5(5)	0.0	24.7(6)	0.47(13)	0.0	0.05(3)	8.26(43)	6.18(28)	0.73(8)	0.0	99.89
		Pig(3)	4	51.4(5)	0.57(12)	1.54(18)	23.8(5)	0.85(5)	16.9(3)	4.80(26)	0.08(5)	0.0	0.0	99.94

Starting Composition: AG8-4

911	1125	Glass(57)	5	59.4(5)	1.44(14)	12.8(1)	11.6(4)	0.34(4)	1.83(14)	5.44(5)	3.56(8)	2.26(3)	0.36(4)	99.03
(96)		Plag(32)	7	59.5(7)	0.15(7)	24.9(4)	0.47(5)	0.0	0.01(2)	7.84(35)	6.12(14)	0.76(7)	0.0	99.74
		Pig(11)	5	50.7(3)	0.52(4)	1.95(19)	24.0(4)	0.76(6)	16.3(6)	5.34(23)	0.13(6)	0.0	0.0	99.70
1074	1075	Glass(60)	4	60.7(8)	1.10(16)	15.3(1)	8.71(55)	0.31(7)	1.15(13)	5.97(24)	4.09(21)	2.10(6)	0.41(11)	99.84
(192)		Plag(25)	5	59.6(5)	0.0	23.9(3)	0.67(16)	0.0	0.03(3)	7.80(39)	5.94(15)	0.79(7)	0.0	98.79
		Pig(15)	5	51.4(4)	0.47(13)	1.48(14)	25.0(4)	0.75(3)	16.0(7)	5.05(10)	0.06(3)	0.0	0.0	100.21

Forced Saturation Experiments at 8 kbar

AT-1+Mix

802	1250	Glass	7	48.7(3)	0.69(19)	17.2(5)	9.69(29)	0.09(3)	8.51(62)	11.6(2)	2.63(15)	0.44(2)	0.12(4)	99.67
(24)		Plag	4	51.1(10)	0.0	29.5(10)	0.66(49)	0.11(9)	0.49(37)	14.6(5)	3.07(17)	0.16(3)	0.0	99.69
		Oliv	6	40.1(4)	0.0	0.0	15.5(10)	0.24(6)	45.0(8)	0.37(2)	0.0	0.0	0.0	101.21
		Aug	7	51.2(9)	0.33(19)	7.25(93)	5.89(62)	0.16(8)	17.7(6)	17.5(8)	0.44(10)	0.0	0.0	100.47
805	1200	Glass	8	48.2(2)	0.98(8)	16.7(4)	9.83(19)	0.17(3)	8.13(19)	11.8(3)	2.64(16)	0.42(4)	0.23(4)	99.10
(24)		Plag	6	50.5(4)	0.10(6)	29.5(3)	0.39(7)	0.0	0.09(2)	15.0(4)	3.12(15)	0.15(2)	0.0	98.85
		Oliv	6	39.8(4)	0.0	0.0	16.2(3)	0.19(5)	44.2(3)	0.46(6)	0.0	0.0	0.0	100.85
		Aug	4	50.5(5)	0.55(7)	7.06(78)	5.25(28)	0.13(6)	16.5(5)	18.9(8)	0.33(6)	0.0	0.0	99.22
808	1200	Glass	9	47.8(5)	1.21(19)	15.9(2)	11.3(3)	0.25(5)	7.17(17)	11.5(1)	2.77(18)	0.55(3)	0.19(4)	98.64
(96)		Plag	5	51.4(8)	0.0	29.9(3)	0.27(7)	0.0	0.05(3)	14.1(3)	3.31(6)	0.18(2)	0.0	99.21
		Oliv	4	38.4(5)	0.0	0.0	19.8(4)	0.35(5)	40.4(4)	0.51(7)	0.0	0.0	0.0	99.46
		Aug	6	52.2(6)	0.63(16)	6.75(26)	6.36(33)	0.20(5)	15.6(3)	19.2(3)	0.26(8)	0.0	0.0	99.20
816[1]	1200	Glass	9	48.3(6)	1.22(12)	16.2(1)	10.4(3)	0.31(10)	7.79(15)	11.9(1)	2.69(21)	0.49(2)	0.15(7)	99.45
(72)														
817	1200	Glass	7	49.1(5)	1.33(17)	16.0(1)	11.1(1)	0.23(5)	6.72(11)	10.5(1)	3.37(20)	0.80(3)	0.20(5)	99.35
(72)														
818	1200	Glass	8	47.4(6)	1.53(23)	15.8(2)	12.8(3)	0.30(7)	6.59(14)	11.0(1)	3.06(10)	0.71(4)	0.19(7)	99.38
(72)														

M-46+Mix

813	1200	Glass	7	49.2(4)	1.05(19)	16.0(1)	10.6(3)	0.14(3)	7.68(15)	11.2(1)	2.71(5)	0.57(3)	0.15(4)	99.30
(48)														
819	1200	Glass	6	48.4(5)	1.16(15)	15.6(1)	12.7(3)	0.30(10)	7.25(13)	10.8(1)	2.65(6)	0.54(4)	0.16(4)	99.56
(72)		Plag	8	50.9(5)	0.0	29.8(3)	0.44(10)	0.0	0.17(4)	14.1(1)	3.30(13)	0.16(2)	0.0	98.87
		Oliv	7	38.6(5)	0.0	0.0	21.1(9)	0.36(8)	40.5(8)	0.40(4)	0.0	0.0	0.0	100.96
		Aug	7	50.7(7)	0.64(11)	6.10(11)	7.50(46)	0.18(4)	16.5(9)	17.6(8)	0.36(5)	0.0	0.0	99.58
869	1150	Glass	8	49.0(1)	2.13(20)	14.3(1)	14.6(2)	0.11(5)	5.12(21)	8.73(12)	3.11(6)	1.14(3)	0.33(5)	98.57
(96)		Plag	5	55.2(9)	0.0	26.9(4)	0.59(22)	0.0	0.15(7)	10.7(6)	4.69(15)	0.50(5)	0.0	98.73
		Aug	5	52.1(7)	0.36(9)	2.75(38)	13.8(8)	0.37(3)	18.1(10)	12.1(15)	0.38(9)	0.0	0.0	99.96
		Pig	5	52.2(5)	0.44(20)	2.52(65)	15.5(6)	0.42(13)	19.7(13)	8.59(16)	0.40(14)	0.0	0.0	99.77

AT-29+Mix

814	1200	Glass	7	49.7(4)	1.20(11)	15.6(2)	12.0(3)	0.26(6)	6.15(12)	9.51(18)	3.04(19)	1.32(4)	0.19(7)	99.97
(48)														

Appendix Table 1. *Continued*

Run (hrs.)	Temp. °C (log fO2)	Phase (mode)	n	SiO2	TiO2	Al2O3	FeO*	MnO	MgO	CaO	Na2O	K2O	P2O5	Total
							2 kbar Experiments							
	Starting Composition:	AT-1												
1234	1120	Glass(32)	10	56.3(12)	2.43(25)	14.0(4)	6.87(99)	0.31(12)	4.19(33)	7.49(38)	3.75(26)	1.49(8)	0.44(7)	97.27
(35)	(-8.8)	Plag(59)	5	54.0(15)	0.0	28.0(6)	0.50(3)	0.0	0.18(5)	11.8(8)	4.61(45)	0.26(3)	0.0	99.35
		Oliv(9)	4	39.8(3)	0.23(7)	0.19(6)	17.5(8)	0.69(6)	42.5(5)	0.39(3)	0.0	0.0	0.0	101.30
		Aug(1)	4	51.0(2)	1.85(12)	3.07(33)	7.53(53)	0.55(10)	16.5(4)	18.1(6)	0.36(6)	0.0	0.0	98.96
		H2O content of melt:		1.8%[2]		Iron Loss 66%[3]								
1180	1100	Glass(44)	5	55.7(8)	1.99(17)	15.8(9)	5.87(30)	0.19(7)	3.66(37)	7.44(25)	3.97(9)	1.42(16)	0.38(6)	96.42
(24)	(-9.5)	Plag(47)	4	52.9(4)	0.0	29.4(5)	0.57(11)	0.0	0.15(3)	12.6(4)	4.08(29)	0.16(3)	0.0	99.86
		Oliv(7)	4	39.2(3)	0.12(12)	0.38(23)	19.0(8)	0.75(6)	41.1(5)	0.43(13)	0.0	0.0	0.0	100.98
		Aug(2)	4	50.4(5)	1.55(12)	4.50(37)	6.66(19)	0.40(9)	15.6(6)	19.0(10)	0.52(13)	0.0	0.0	98.63
		H2O content of melt:		1.8%		Iron Loss: 43%								
	Starting Composition:	AT-112												
1162	1060	Glass(6)	5	59.5(5)	1.61(6)	15.2(5)	6.38(46)	0.24(7)	2.26(10)	5.95(4)	3.71(27)	1.58(11)	0.30(6)	96.73
(24)	(-9.5)	Plag(66)	5	53.5(7)	0.0	29.2(7)	0.57(11)	0.0	0.05(4)	12.8(6)	4.11(20)	0.20(4)	0.0	100.43
		Oliv(13)	4	37.8(6)	0.16(5)	0.0	28.7(7)	0.67(13)	32.9(1)	0.34(4)	0.0	0.0	0.0	100.57
		Aug(16)	4	51.6(3)	0.95(13)	2.84(41)	9.69(12)	0.41(2)	14.4(4)	19.2(3)	0.39(19)	0.0	0.0	99.48
		H2O content of melt:		1.8%		Iron Loss: 43%								
	Starting Composition:	AT-29												
1165	1060	Glass(63)	7	59.9(9)	1.28(15)	15.2(2)	6.90(4)	0.25(6)	2.24(11)	5.46(10)	3.58(16)	2.44(7)	0.38(12)	97.63
(24)	(-9.5)	Plag(28)	5	57.1(5)	0.0	27.0(2)	0.73(8)	0.0	0.05(4)	10.3(3)	4.92(16)	0.50(3)	0.0	100.60
		Aug(4)	5	51.9(6)	0.55(10)	1.86(16)	11.1(4)	0.55(11)	14.6(4)	19.3(3)	0.39(7)	0.0	0.0	100.25
		Opx(4)	5	53.8(6)	0.34(12)	1.38(59)	17.0(2)	0.61(4)	24.6(3)	2.25(13)	0.14(8)	0.0	0.0	100.12
		H2O content of melt:		1.8%		Iron Loss: 30%								
1148	1020	Glass(54)	5	60.0(3)	1.12(10)	15.3(3)	6.72(30)	0.13(4)	1.32(11)	4.34(17)	3.79(22)	3.26(5)	0.28(7)	96.26
(24)	(-9.9)	Plag(33)	5	56.3(3)	0.0	26.5(5)	0.95(15)	0.0	0.01(2)	10.5(4)	5.13(28)	0.52(4)	0.0	99.91
		Aug(7)	5	51.9(7)	0.69(7)	1.68(16)	11.0(4)	0.31(9)	14.3(2)	19.3(5)	0.37(9)	0.0	0.0	99.55
		Opx(6)	4	53.7(7)	0.50(4)	0.86(18)	20.3(1)	0.73(18)	22.6(5)	2.02(7)	0.10(7)	0.0	0.0	100.81
		H2O content of melt:		1.8%		Iron Loss: 17%								
1174	1020	Glass(43)	4	66.1(13)	0.77(26)	13.4(4)	3.66(10)	0.07(7)	0.65(9)	2.45(15)	3.69(3)	3.62(3)	0.23(7)	94.64
(96)	(-10.3)	Plag(42)	5	55.5(10)	0.0	28.2(6)	0.74(28)	0.0	0.03(4)	11.4(4)	4.61(23)	0.40(9)	0.0	100.88
		Aug(8)	5	51.6(10)	0.48(19)	1.98(27)	11.2(5)	0.52(13)	14.5(2)	19.3(5)	0.25(4)	0.0	0.0	99.83
		Opx(8)	3	53.2(2)	0.40(16)	0.82(36)	19.7(6)	0.83(13)	23.0(3)	2.03(9)	0.06(11)	0.0	0.0	100.04
		H2O content of melt:		1.9%		Iron Loss: 56%								
1249	1020	Glass(75)	5	58.8(5)	1.19(12)	16.2(1)	4.32(11)	0.20(3)	2.50(7)	4.85(8)	3.91(22)	2.64(4)	0.25(5)	94.86
(96)	(-10.3)	Plag(8)	4	52.5(4)	0.0	29.3(21)	0.52(6)	0.0	0.08(4)	12.8(2)	3.78(18)	0.28(2)	0.0	99.26
		Aug(8)[4]	4	51.8(2)	0.72(22)	2.06(23)	8.13(22)	0.40(7)	16.4(1)	19.3(3)	0.08(5)	0.0	0.0	98.89
		H2O content of melt:		1.8%		Iron Loss: 40%								
704	1000	Glass(43)	5	65.2(5)	1.11(10)	14.6(3)	2.07(13)	0.08(7)	0.92(10)	2.46(18)	4.06(1)	4.10(9)	0.26(5)	94.85
(96)	(-11.8)	Plag(41)	4	56.5(11)	0.0	27.0(8)	0.68(10)	0.0	0.02(2)	10.2(4)	5.21(27)	0.49(4)	0.0	100.10
		Aug(11)	5	51.8(8)	0.47(14)	1.88(41)	10.5(8)	0.45(14)	14.7(2)	19.4(4)	0.39(5)	0.0	0.0	99.59
		Opx(5)	1	53.2	0.32	1.44	15.4	1.02	25.0	2.46	0.26	0.0	0.0	99.10
		H2O content of melt:		2.0%		Iron Loss: 73%								
	Starting Composition:	AT-25												
1164	1060	Glass(69)	9	61.5(11)	1.09(15)	15.7(2)	5.47(30)	0.11(6)	2.06(14)	4.90(36)	3.60(15)	2.87(5)	0.21(6)	97.51
(24)	(-9.5)	Plag(22)	6	54.0(5)	0.0	29.5(4)	0.65(10)	0.0	0.09(3)	12.3(5)	4.07(17)	0.33(4)	0.0	100.94
		Oliv(3)	4	36.6(10)	0.0	0.0	26.2(11)	0.48(2)	34.5(7)	0.36(7)	0.0	0.0	0.0	98.14
		Aug(5)	7	51.0(5)	0.61(8)	1.86(54)	10.2(13)	0.36(12)	14.8(5)	19.9(8)	0.31(6)	0.0	0.0	99.04
		H2O content of melt:		1.9%		Iron Loss: 59%								
1173	1020	Glass(43)	5	68.4(8)	1.21(35)	14.2(4)	2.13(19)	0.20(7)	0.85(14)	2.31(28)	3.73(25)	3.98(11)	0.18(19)	97.19
(96)	(-10.3)	Plag(43)	4	55.7(4)	0.0	28.1(8)	0.41(14)	0.0	0.07(4)	11.4(3)	4.61(22)	0.45(4)	0.0	100.74
		Aug(8)	5	51.8(6)	0.40(11)	1.84(37)	9.71(54)	0.49(10)	15.1(4)	19.8(7)	0.26(7)	0.0	0.0	99.40
		Opx(7)	4	53.8(8)	0.26(21)	1.09(28)	17.2(16)	0.58(17)	25.1(8)	1.93(33)	0.01(2)	0.0	0.0	99.97
		H2O content of melt:		1.9%		Iron Loss: 24%								
1147	1020	Glass(60)	4	60.6(2)	1.00(19)	16.0(4)	5.56(23)	0.14(1)	1.80(18)	4.47(32)	3.61(20)	3.58(9)	0.18(5)	96.94
(24)	(-9.9)	Plag(28)	6	57.0(6)	0.0	27.6(4)	0.63(4)	0.0	0.02(2)	9.92(34)	5.04(22)	0.61(8)	0.0	100.82
		Oliv(3)	5	38.0(3)	0.11(3)	0.0	29.5(3)	0.58(3)	31.6(8)	0.32(9)	0.0	0.0	0.0	100.11
		Aug(9)	5	52.3(4)	0.57(8)	1.46(15)	10.8(2)	0.51(11)	14.1(3)	19.5(3)	0.19(3)	0.0	0.0	99.43
		H2O content of melt:		1.8%		Iron Loss: 14%								
1248	1020	Glass(70)	6	58.7(8)	1.13(19)	16.5(6)	5.60(69)	0.14(9)	1.56(14)	4.55(29)	3.88(15)	3.61(17)	0.25(12)	95.92
(96)	(-10.3)	Plag(19)	6	57.0(6)	0.0	28.1(5)	0.74(10)	0.0	0.04(2)	11.5(5)	4.40(42)	0.49(6)	0.0	98.97
		Oliv(3)	5	36.3(4)	0.10(8)	0.18(8)	33.2(4)	0.60(15)	29.1(5)	0.35(4)	0.0	0.0	0.0	99.83
		Aug(8)	5	51.4(3)	0.53(5)	1.77(26)	10.2(4)	0.37(9)	14.6(3)	20.0(2)	0.29(10)	0.0	0.0	99.16
		H2O content of melt:		1.8%		Iron Loss: 14%								
							5 kbar Experiments							
	Starting Composition:	AT-29												
1287	1060	Glass(74)	5	57.2(9)	1.20(14)	15.7(2)	6.58(36)	0.19(4)	2.13(12)	5.31(16)	3.85(14)	2.51(9)	0.27(4)	94.94
(103)	(-9.6)	Plag(17)	4	54.3(12)	0.0	28.2(4)	0.63(6)	0.0	0.07(2)	11.4(2)	4.66(22)	0.41(7)	0.0	99.67
		Aug(6)	4	50.4(5)	0.75(9)	3.38(87)	11.6(2)	0.40(8)	14.1(2)	18.4(6)	0.33(9)	0.0	0.0	99.36
		Opx(3)	3	53.0(5)	0.24(10)	1.12(8)	18.8(3)	0.56(9)	23.3(5)	2.18(7)	0.07(2)	0.0	0.0	99.27
		H2O content of melt:		1.8%		Iron Loss: 29%								
	Starting Composition:	AT-25												
1286	1060	Glass(48)	5	62.4(6)	1.88(28)	15.2(4)	4.29(25)	0.16(5)	1.10(8)	3.08(17)	4.21(24)	4.65(14)	0.52(4)	97.49
(103)	(-9.6)	Plag(35)	5	56.4(7)	0.0	27.2(3)	0.31(4)	0.0	0.05(3)	9.99(14)	5.18(12)	0.78(4)	0.0	99.91
		Aug(4)	1	49.9	0.71	1.40	10.6	0.21	15.8	15.9	0.27	0.0	0.0	97.53
		Opx(3)	2	52.3(9)	0.57(11)	2.86(24)	19.0(12)	0.32(16)	23.1(7)	2.17(4)	0.01(1)	0.0	0.0	100.33
		H2O content of melt:		2.0%		Iron Loss: 41%								
	Starting Composition:	P-22+Mix												
1324	1100	Glass(48)	7	52.9(6)	1.90(19)	18.92(37)	2.38(13)	0.0	5.85(29)	8.22(24)	3.59(19)	0.57(7)	0.25(9)	94.58
(24)	(-8.6)	Plag(18)	2	50.9(2)	0.0	31.2(1)	0.17(12)	0.0	0.22(1)	13.0(3)	4.16(7)	0.09(3)	0.0	99.74
		Oliv(5)	3	39.5(4)	0.0	0.0	8.2(13)	0.0	50.1(18)	0.18(2)	0.0	0.0	0.0	97.96
		Aug(30)	4	52.2(10)	0.76(27)	4.3(15)	3.31(62)	17.4(13)	20.3(5)	0.41(2)	0.0	0.0	0.0	98.68
		H2O content of melt:		1.7%		Iron Loss: 83%								

Note: Explanation of column headings:

Run (hrs.) — Run number, below which in parentheses is listed the run duration in hours. Two duration values separated by a slash indicate a crystallization experiment; the rock was melted at high temperatures for the first duration then crystallized at lower temperatures for the second.

Temp., °C (log f_{O_2}) — Temperature of the experiment; for crystallization experiments the two temperatures, corresponding to the duration at each temperature, are separated by a slash. Below the temperature(s), the oxygen fugacity of the experiment is listed in parentheses for the 1-atm, 2-kbar, and 5-kbar experiments.

Appendix Table 1. *Continued*

Phase (mode)	The phases observed in the run products are listed, followed by the weight percent mode of each phase in the experiment (in parentheses; corrected for Fe loss in the 2- and 5-kbar experiments). See text for method of calculation.
n	Number of analyses of each phase used to calculate mean and standard deviations of analyses.

The remaining columns are the oxide analyses of the run products. The mean value of the analyses is given followed by the standard deviation of analyses in terms of the smallest units recorded; thus 51.4(4) is read as 51.4 ± 0.4 wt%. Where a value of 0.0 is given, that oxide was not determined. $FeO^* =$ total Fe given as FeO.

[1] Melts produced in experiments 813, 814, 816, 817, and 818 coexist with plagioclase, olivine, and augite.

[2] H_2O content of melt calculated by method discussed in text.

[3] Loss of Fe relative to initial bulk-rock Fe content.

[4] Orthopyroxene was optically identified, but not analyzed with the electron microprobe.